

Sensor and Simulation Notes

Note 164

December 1972

CLEARED
FOR PUBLIC RELEASE
PL/PH 16 DEC 96

Study of a Charged Wire Grid for Reducing
Electron Backscatter in EMP Satellite Simulators

F. M. Tesche
The Dikewood Corporation
Albuquerque, New Mexico

Abstract

This note presents a brief study of a wire grid designed to reduce electron backscatter within an EMP satellite simulator. The grid, which is maintained at a constant potential, is modeled by an infinite number of thin cylinders which are located parallel to a perfectly conducting plane at zero potential. The distribution of potential around and away from the grid is shown for one particular grid geometry, as are the trajectories for electrons being emitted into the grid region from the ground plane. Curves showing the fraction of electrons escaping to infinity as a function of the angle of departure and the initial kinetic energy are presented for various grid geometries and an indication as how to use this data in subsequent investigation is outlined.

DL 910-11970

ACKNOWLEDGMENT

I wish to thank Dr. Carl Baum for his discussions regarding this problem, as well as Drs. Kelvin Lee and Lennart Marin at Dikewood/Westwood for their comments. Thanks are also due to Mrs. Zoe Lynda Pine for computational assistance, and to Rosemary Lovato and Susan Bonilla for preparing the manuscript.

I. INTRODUCTION

In a recent note,⁽¹⁾ Baum describes the general configuration of an EMP Satellite Simulator. This class of simulators is designed to study the effects of system generated EMP which is produced by a flux of gamma and X-rays impinging on a satellite in space as in Fig. 1. The proposed simulator shown in Fig. 2 consists of a large vacuum tank which surrounds the satellite under test. The photon beam is produced externally to the cavity, passes into the vacuum chamber and produces Compton electrons from the satellite surface. These electrons travel about in the space near the satellite, creating large currents which produce the radiated electromagnetic fields.

As pointed out by Baum, some of the Compton electrons may escape to the cavity wall, be absorbed and cause secondary electrons to be emitted back to the satellite under test. In addition, part of the incident photon flux may cause Compton electrons to be emitted from the cavity walls and travel back to the satellite. As these effects are not present in the case of the actual satellite in free space, it is desirable to reduce their contributions in the simulated test.

One possible method of reducing such "spurious electrons" would be to place a wire mesh or grid slightly away from the cavity wall. By biasing the grid to a large negative potential with respect to the wall, the electrons emitted from the wall feel a decelerating force, which prevents the electrons from continuing on to the satellite, as indicated in Figure 3.

This note investigates the properties of such a wire grid. Of special interest in this problem will be the potential distributions around the grids, and a study of the behavior of the electrons which are emitted from the wall with a fixed kinetic energy and in a specified direction, as a function of grid spacing, location and applied potential.

One possible model of the cavity wall and repelling grid is to consider the structure to be locally flat and replace it by an infinite

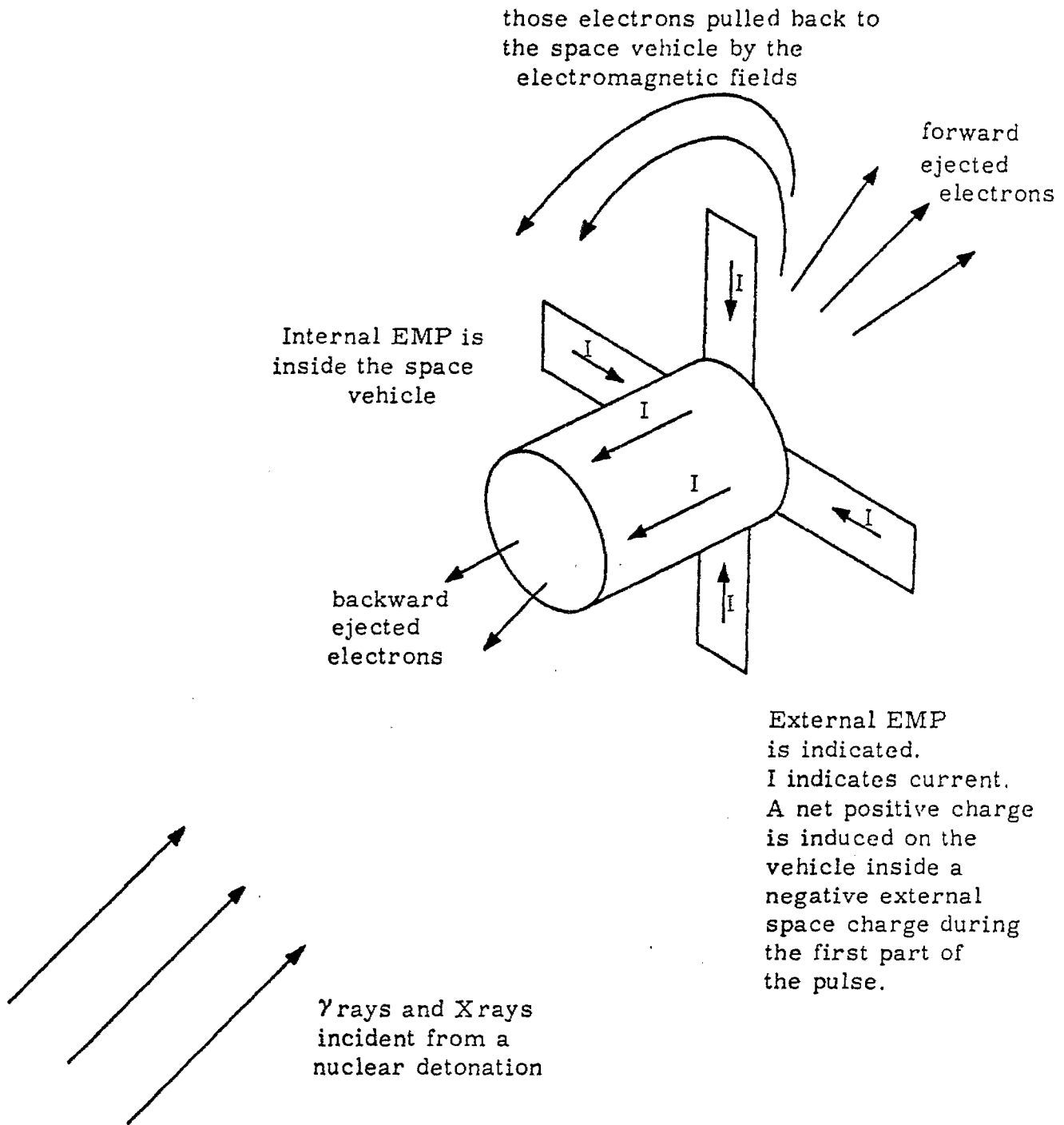


Figure 1. System Generated EMP on a Space Vehicle

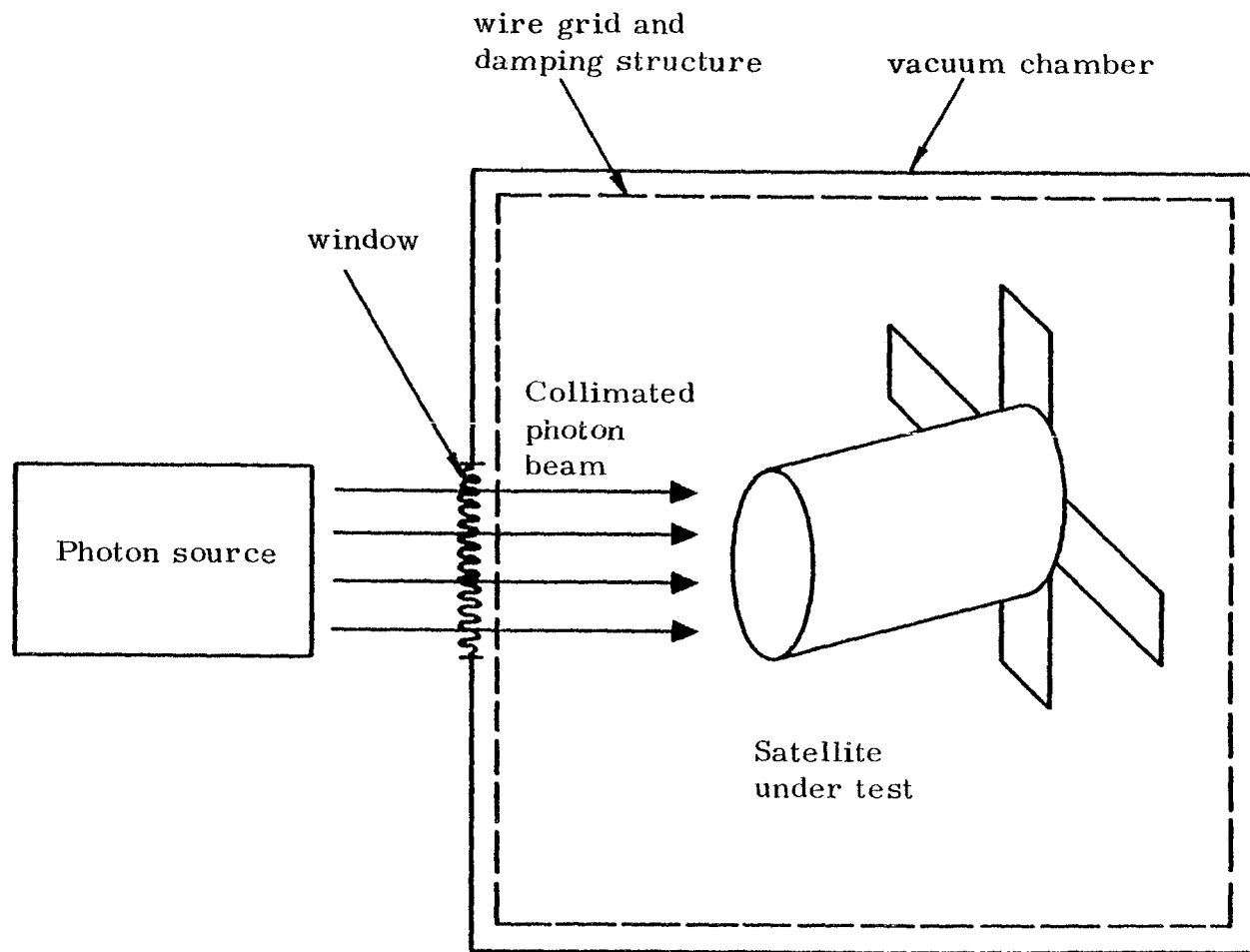


Figure 2. General Lay-out of the EMP Satellite Simulator

The potential on this side is negative (almost $-V$) with respect to the tank wall.

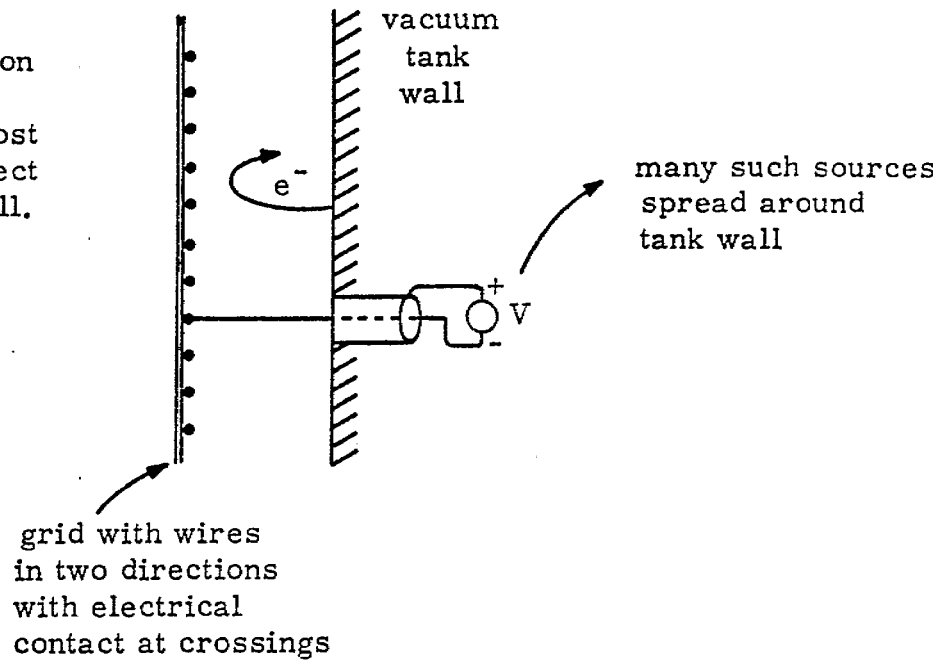


Figure 3. Single negative grid near vacuum tank wall

conducting plane at potential $\Phi = 0$, with a grid of cylindrical wires a distance b above the plane, which has a potential $\Phi = -V_0$. The distance separating the wire grids is given by $2a$ and the value of the wire radius is r_0 .

For simplicity, the wire grid is assumed to be uniform in one direction, thereby reducing the problem to the two dimensional geometry as shown in Figure 4. Moreover, it will be assumed that the wire radius is very small compared with the other distances involved in the problem, such as wire spacing. This enables one to use the approximation that the wire can be represented by a line charge of vanishing radius, so as to simplify the formulation which is presented in the next section.

In Section III, the trajectories of electrons leaving the plate with given initial conditions are determined. These results help in quantifying the shielding properties of this grid structure. Specifically, the fraction of electrons escaping to infinity for a given initial kinetic energy and angle of emission from the plate is presented for various b/a ratios.

II. EVALUATION OF THE POTENTIAL

Using the idealized structure as shown in Figure 4, it is noted that there is a periodicity in the \hat{y} direction so that it is necessary to consider the solution of the problem only in one of the unit cells shown in Figure 5. Replacing the cylinder of radius r_0 by a line charge ζ_0 (whose value will be determined later), the task is to find the potential Φ in the region $x > 0$ and $-a < y < a$. Dividing this region into two sub-regions, I and II, it is seen that the boundary conditions that Φ must obey are as follows:

Region I

$$\Phi_I(0, y) = 0 \quad (1)$$

$$\left. \frac{\partial \Phi_I}{\partial y}(x, y) \right|_{y=\pm a} = 0 \quad (2)$$

Region II

$$\lim_{x \rightarrow \infty} \Phi_{II}(x, y) = \text{const.} \quad (3)$$

$$\left. \frac{\partial \Phi_{II}}{\partial y}(x, y) \right|_{y=\pm a} = 0 \quad (4)$$

Interface

$$\Phi_I(b, y) = \Phi_{II}(b, y) \quad (5)$$

$$\left[\frac{\partial \Phi_I}{\partial x}(x, y) - \frac{\partial \Phi_{II}}{\partial x}(x, y) \right] \Big|_{x=b} = \frac{\zeta_0}{\epsilon_0} \delta(y). \quad (6)$$

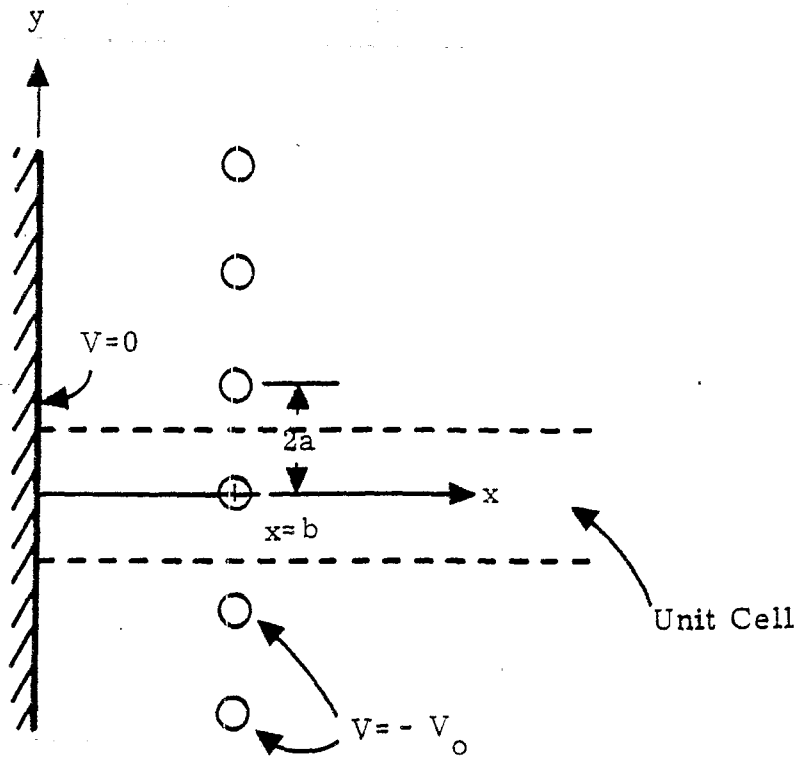


Figure 4. Geometry of the Problem.

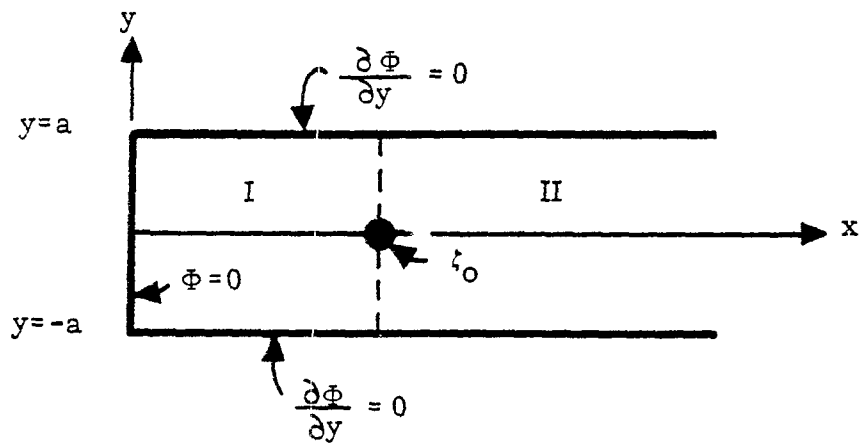


Figure 5. Unit Cell and Boundary Conditions for Φ .

Since regions I and II are free of charge, the potentials there are solutions to Laplace's equation

$$\nabla^2 \Phi(x, y) = 0 \quad (7)$$

Using the standard technique of separation of variables, the representations for the potential in the two regions take the following forms:

$$\Phi_I(x, y) = \frac{\zeta_0}{a\epsilon_0} \left[\frac{x}{2} + \sum_{n=1}^{\infty} \frac{1}{\gamma_n} \cos(\gamma_n y) e^{-\gamma_n b} \sinh(\gamma_n x) \right] \quad x \leq b \quad (8)$$

$$\Phi_{II}(x, y) = \frac{\zeta_0}{a\epsilon_0} \left[\frac{b}{2} + \sum_{n=1}^{\infty} \frac{1}{\gamma_n} \cos(\gamma_n y) e^{-\gamma_n x} \sinh(\gamma_n b) \right] \quad x \geq b \quad (9)$$

where $\gamma_n = n\pi/a$.

Note that as $x \rightarrow \infty$, Eq. (9) gives $\Phi_{II}(x, y) \sim \frac{\zeta_0}{a\epsilon_0} \frac{b}{2}$ for the potential at infinity. Also, as $y \rightarrow 0$ and $x \rightarrow b$, the potential goes to infinity as it should for an infinitesimally thin line charge. For distances very close to the line charge, the summations in (8) and (9) are difficult to sum. Letting $(b-x) = \epsilon$ in Eq. (8) and $(x-b) = \epsilon$ in Eq. (9), and examining the asymptotic behavior of the terms in the respective sums, it may be noted that by adding and subtracting the well-known series

$$c \sum_{n=1}^{\infty} \frac{e^{-jnz}}{n} = -c \ln(1 + e^{-jz}) \quad (10)$$

the resulting series converges much more rapidly. In this case, $c = a/4\pi$ and $z = \pi(\pm y - j\epsilon)/a$.

Another representation for the potential in the unit cell is obtainable from conformal mapping techniques and is employed in a note treating a parallel plate EMP simulator problem. ⁽²⁾

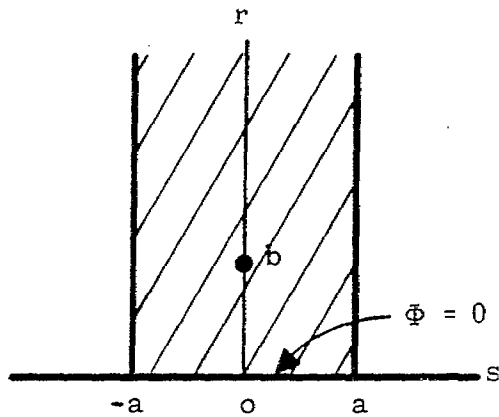
Using the conformal transformation $w = e^{i \frac{\pi}{a} t}$ where $w = u + iv$ and $t = (r + is)$, the periodic strip $s > 0, -a \leq t \leq a$ in Figure 6 is transformed into the unit circle with the boundary condition $\Phi = 0$ on the perimeter. A line charge at $(r, s) = (0, b)$ is transformed into a similar charge at $(u, v) = \left(0, e^{-\frac{\pi b}{a}}\right)$. With this charge location, the potential within the cylinder may be obtained using the method of images. Expressing the answer in terms of the original x, y co-ordinate system of Figure 2, the result is given by

$$\Phi(x, y) = \frac{\zeta_0}{4\pi\epsilon_0} \ln \left[\frac{\cosh(\pi(x+b)/a) - \cos(\pi y/a)}{\cosh(\pi(x-b)/a) - \cos(\pi y/a)} \right]. \quad (11)$$

Note that this expression is clearly more desirable than those of Eqs. (9) and (10), due to the relative ease of numerical evaluation. As $x \rightarrow \infty$, the asymptotic form of this equation is the same as that obtained from the previous equations.

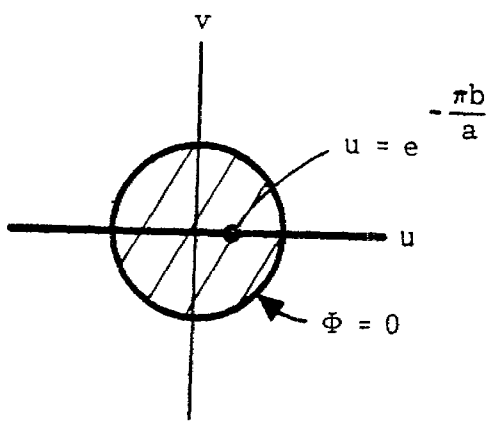
The relation in Eq. (11) may be used to obtain plots of contours of constant potential for various values of b and a . In evaluating such plots, it is convenient to normalize the potential to that at infinity, given by $\Phi_\infty = \frac{\zeta_0}{2\epsilon_0} \left(\frac{a}{b}\right)$. This removes all dependence on the magnitude of the line charge density. Figures 7 through 10 show the normalized constant potential contours for various a/b ratios. Note that away from the wire, the contours are far from being circular in shape, but as one gets closer to the charge, the contours become more like the circular ones obtained from an isolated charge.

One quantity of interest is the variation of the potential as the observation point approaches the line charge. Letting $y = 0$ and the observation point be defined by $x = b - r_0$, plots of the normalized potential Φ/Φ_∞ as a function of r_0/b with a/b as a parameter are given in Figure 11. From these curves, the voltage source needed to place between the ground plane and the wires with radius r_0 , such that Φ at ∞ is unity, can be determined.



$$t = r + is$$

$$\Downarrow w = e^{i \frac{\pi}{a} t}$$



$$w = u + iv$$

Figure 6 Conformal mapping of unit cell into a circle.

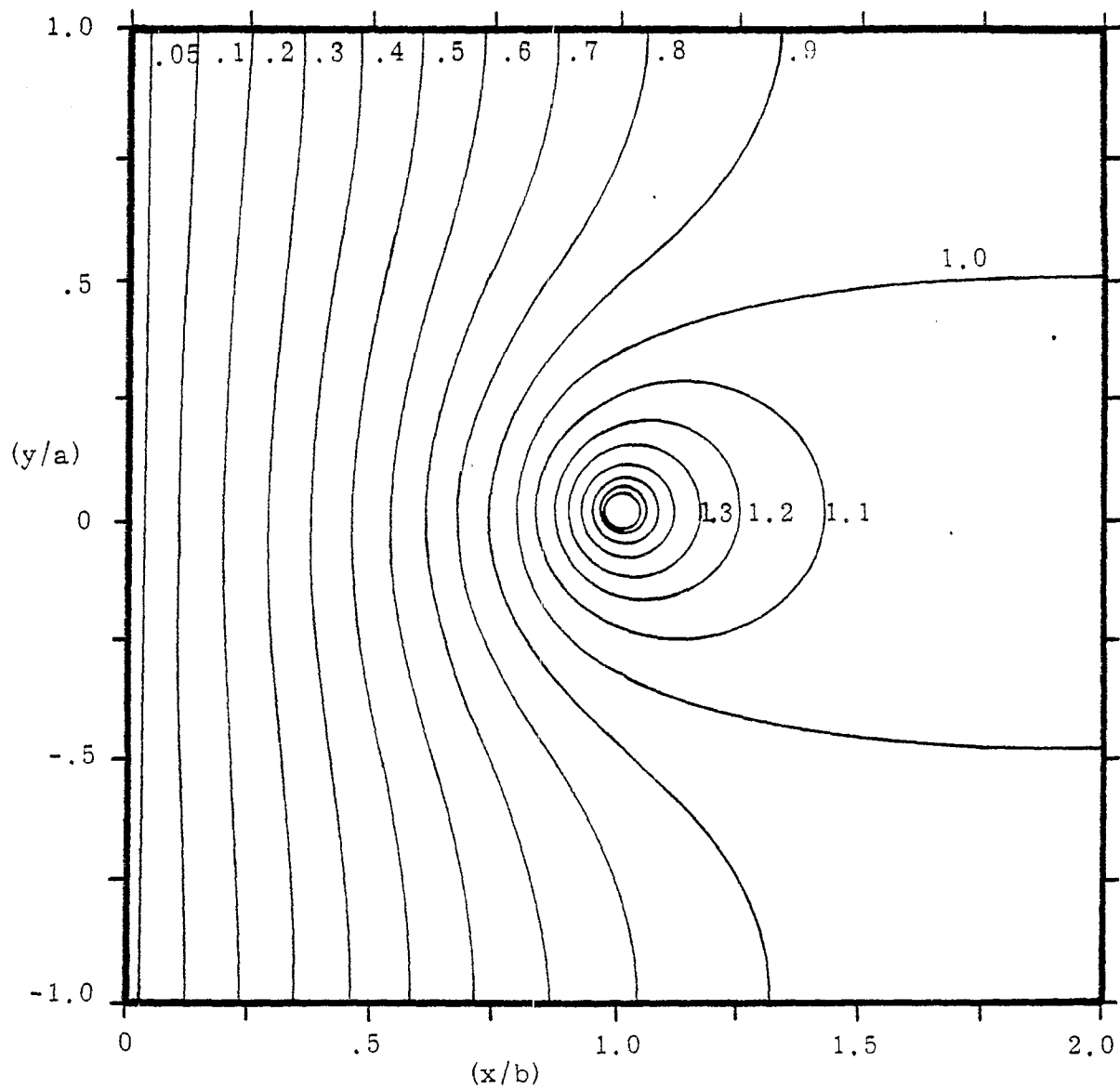


Figure 7. Contour plots of the normalized potential due to a line charge within a unit cell of $a/b = 1$.

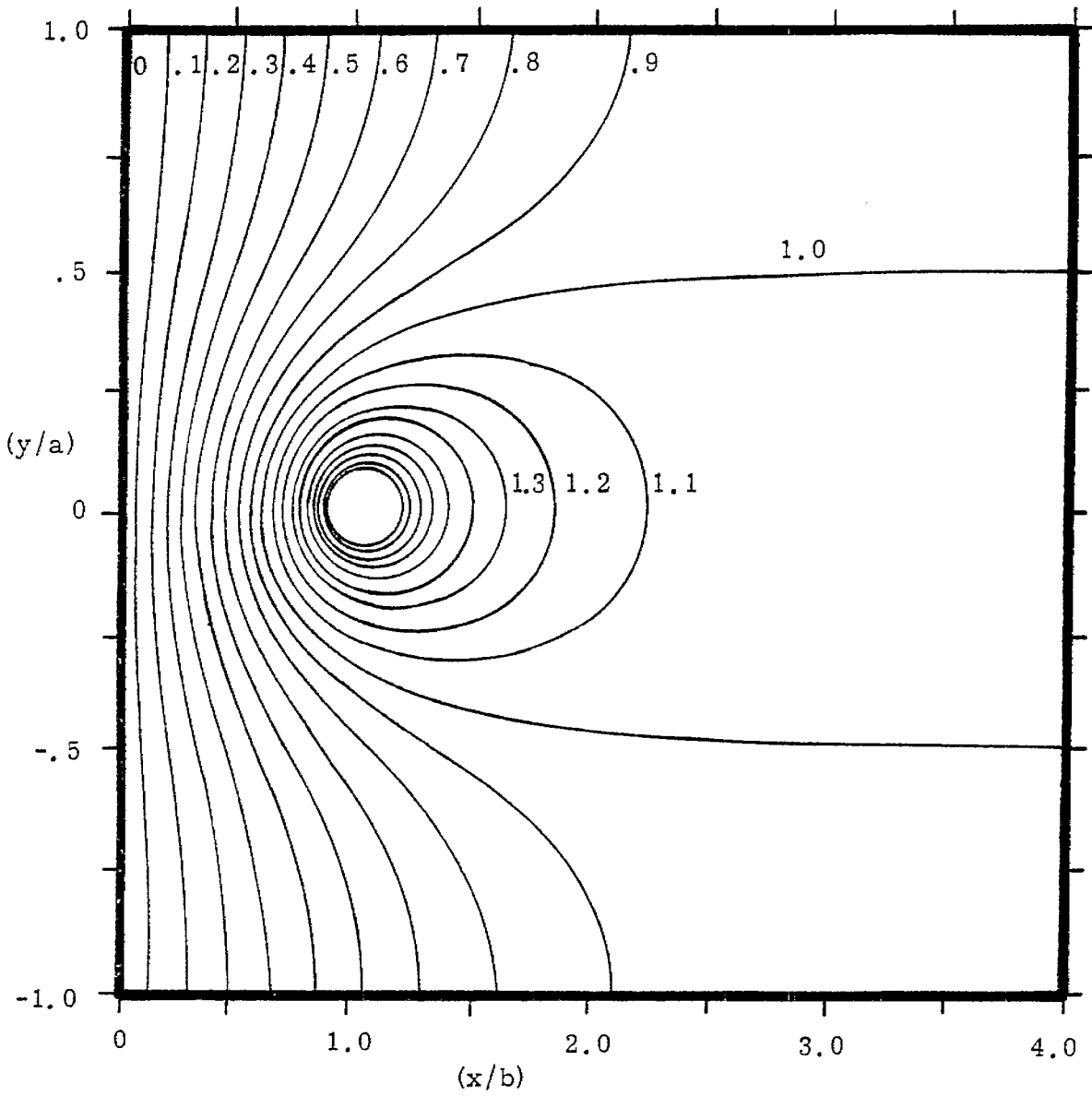


Figure 8. Contour plots of the normalized potential due to a line charge within a unit cell of $a/b = 2$.

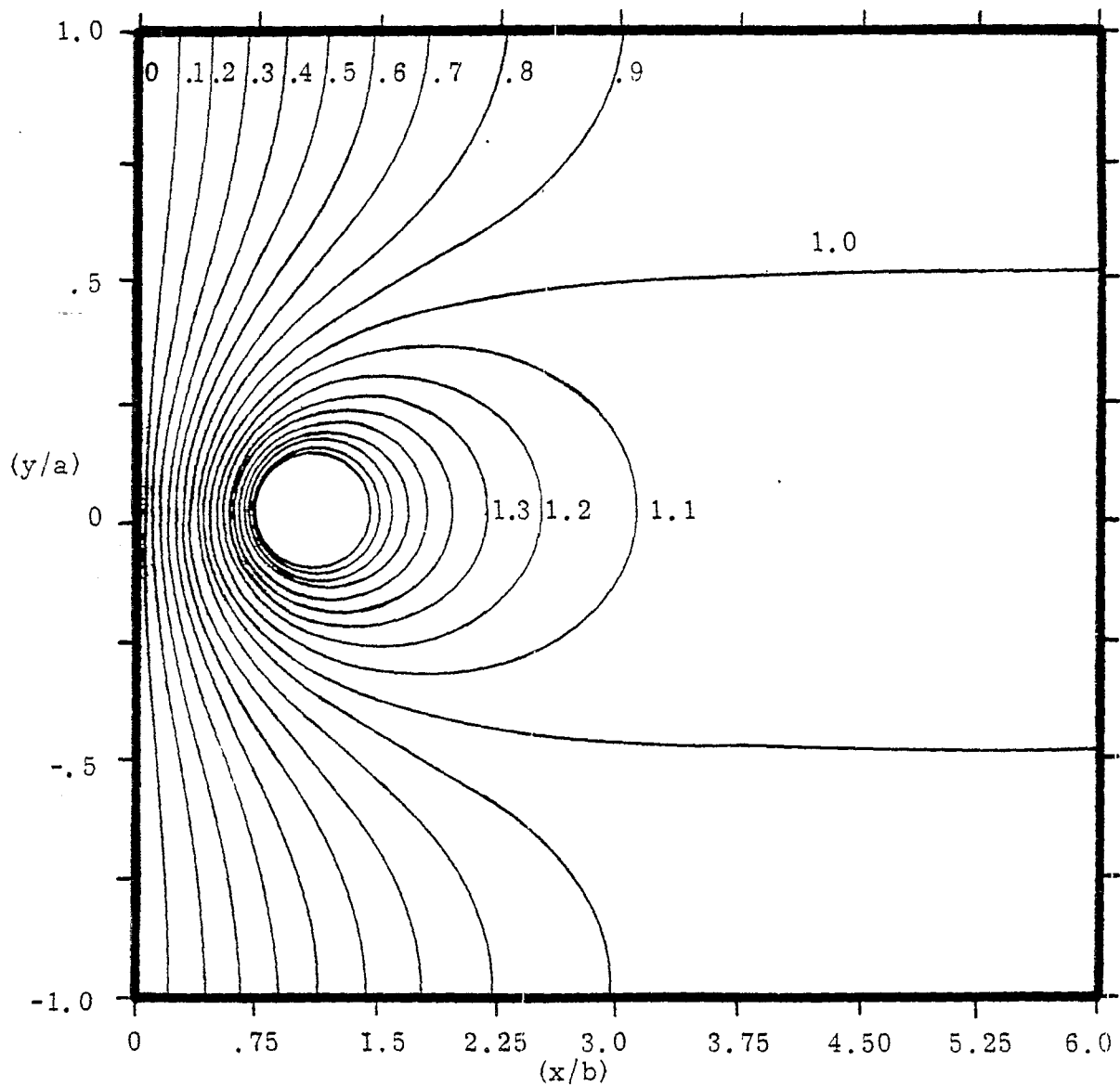


Figure 9. Contour plots of the normalized potential due to a line charge within a unit cell of $a/b = 3$.

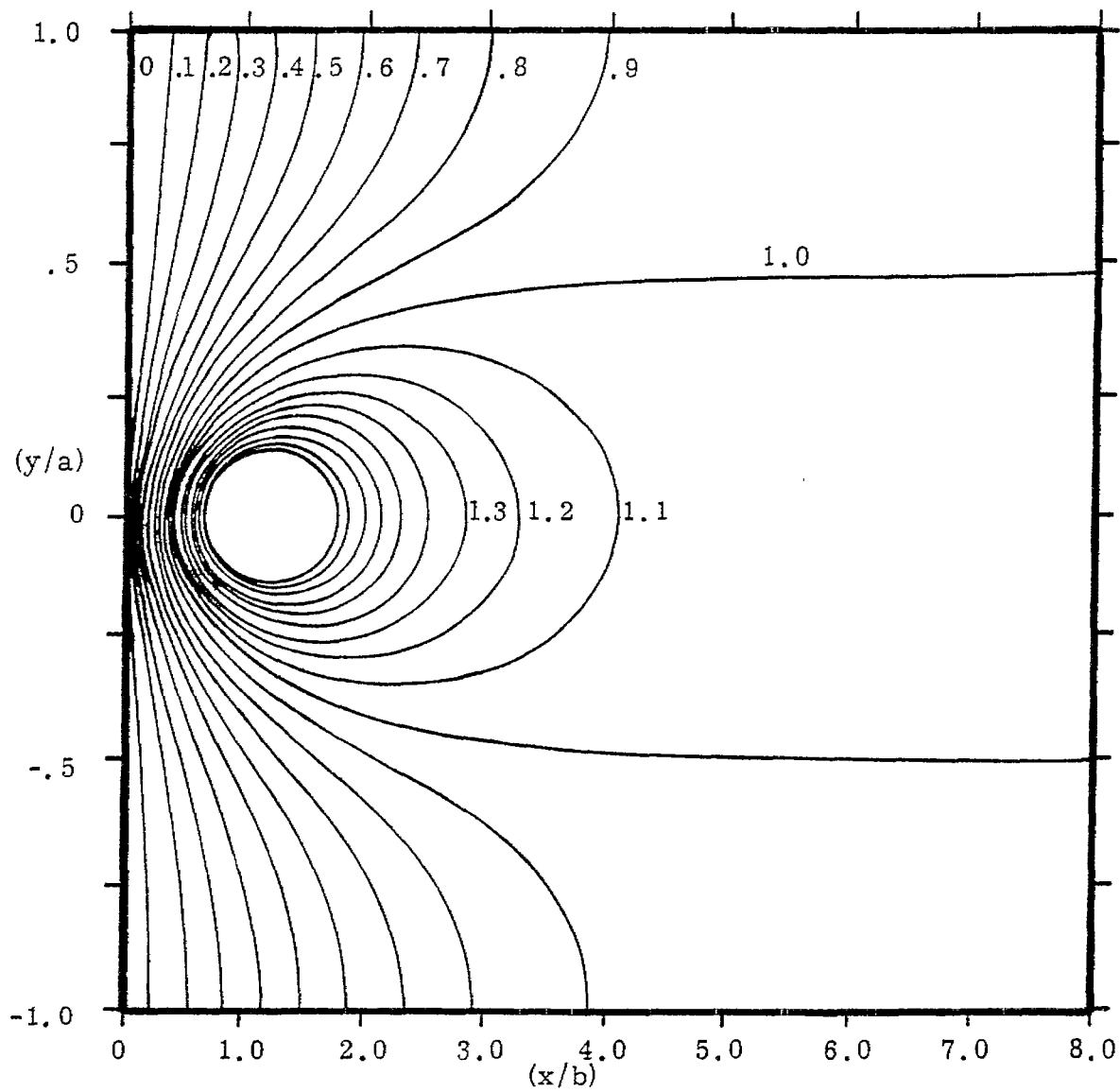


Figure 10. Contour plots of the normalized potential due to a line charge within a unit cell of $a/b = 4$.

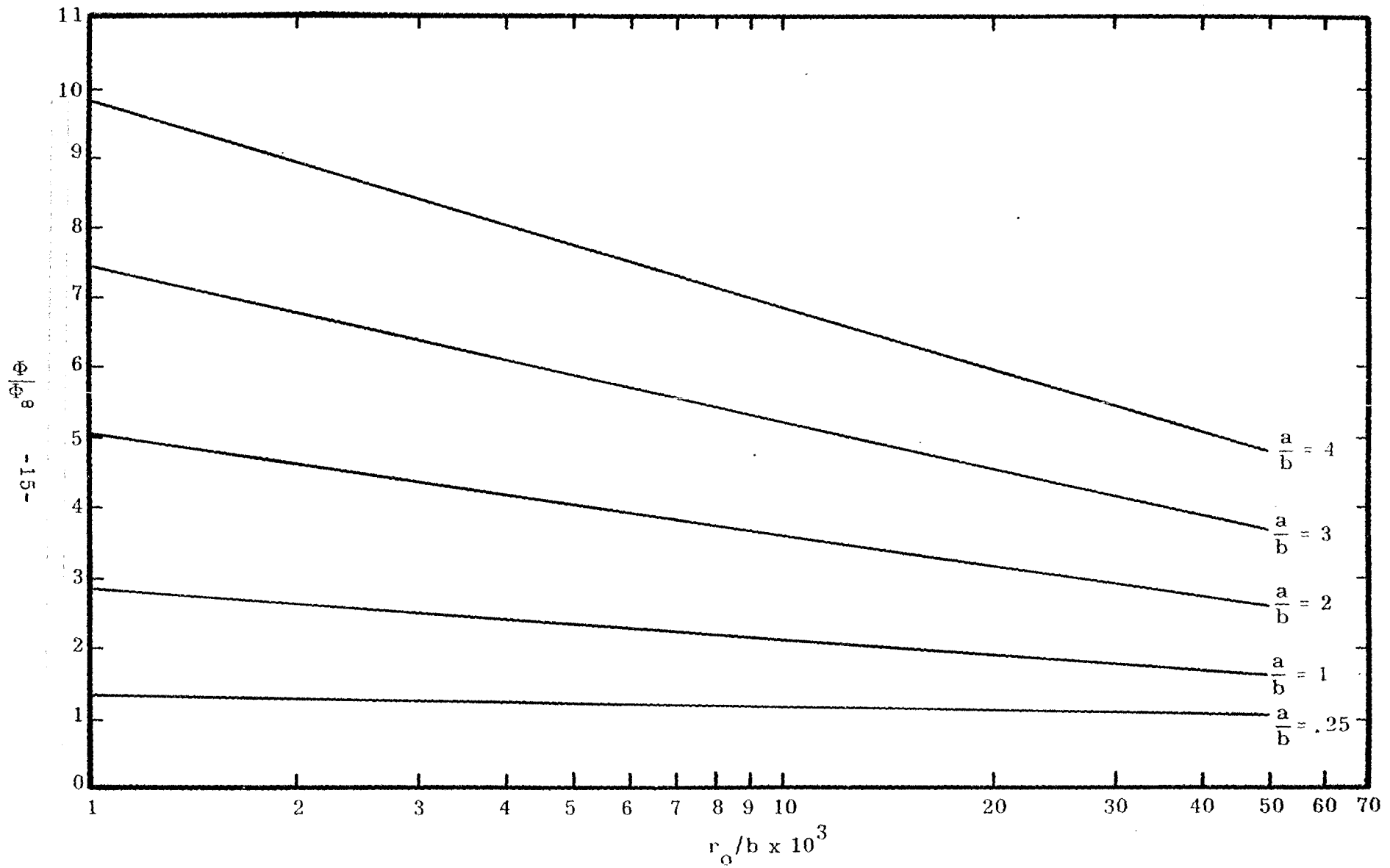


Figure 11. Plots of the normalized potential close to the line charge for various dimensions of the unit cell.

It should be noted that had similar calculations been made for the observation point moving in on the $x = b$ line, slightly different values of the potential for a given r_0 would be obtained, due to the fact that the potential contours are not exactly circular as was previously mentioned. As the point of observation becomes very close to $(x,y) = (b,0)$, this difference becomes negligible and this effect is disregarded in the present analysis.

III. CALCULATION OF ELECTRON TRAJECTORIES

From simply looking at the plots of the potential contours around the wire grid, it is difficult to tell exactly how well the grid will impede the motion of electrons into the working volume of the simulator. One possible way to quantify the shielding properties of the grid is to compute the fraction of electrons which escape to infinity for a given set of assumed initial conditions.

To perform these calculations, it is necessary to know the trajectories that the electrons take after they are emitted from the plate. For the present analysis, several simplifying assumptions will be made; namely, that the electrons are non-relativistic and that space charge effects may be neglected. It will be assumed that the electrons are emitted from the plate with an initial kinetic energy given by T , and in a direction described by the angles θ and ϕ in the usual polar co-ordinate system as shown in Figure 12. For non-relativistic electrons of mass m , the magnitude of the initial electron velocity is given by

$$|v_o| = \sqrt{2T/m} \quad (12)$$

and the cartesian components of the velocity are

$$v_{x_o} = |v_o| \sin\theta \sin\phi \quad (13)$$

$$v_{y_o} = |v_o| \sin\theta \cos\phi \quad (14)$$

$$v_{z_o} = |v_o| \cos\theta \quad (15)$$

To determine the electron trajectory, the equation of motion $\bar{F} = \ddot{\bar{x}}$ must be integrated, subject to the proper initial conditions. Noting that $\bar{F} = q\bar{E} = -q\nabla\Phi$, and choosing an increment in time Δt so small that the

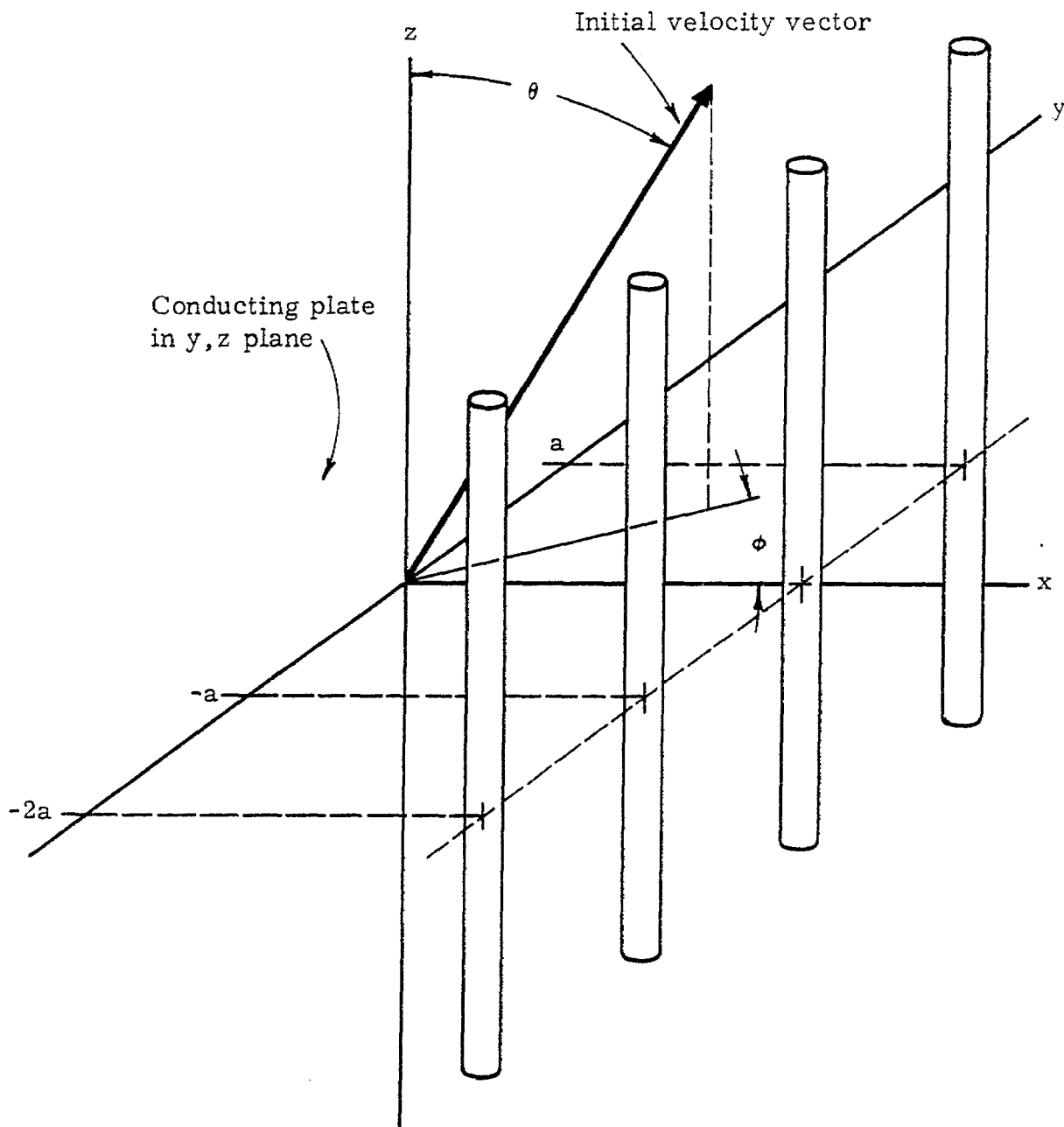


Figure 12. Three-dimensional view of wire grid structure and the co-ordinate system for electron trajectory determination.

force is approximately constant, the equation of motion can be integrated to yield

$$\Delta \bar{x} = \frac{-q}{2m} \nabla \Phi (\Delta t)^2 + \bar{v} (\Delta t) \quad (16)$$

with q representing the electronic charge.

Thus, given an initial position \bar{x}_0 , and velocity \bar{v}_0 , Eq. (16) may be used to determine a new position given by $\bar{x}_1 = \bar{x}_0 + \Delta \bar{x}$. A new velocity is subsequently determined by $\bar{v}_1 = \bar{v}_0 - \frac{q}{m} \nabla \Phi (\Delta t)$ and the procedure can be repeated until the electron either escapes or returns back to the plate.

Using the two-dimensional potential distribution (in the x-y plane) for this problem, it is clear that the velocity v_{z0} is unchanged as the electron moves about in the region away from the ground plane.

For the purposes of illustrating the electron trajectories, consider the case where $\theta = \pi/2$. Since $v_{z0} = 0$, the motion of the electrons takes place in the x,y plane only. Figures 13 through 24 show some typical trajectories for various normalized initial kinetic energies T_n , where

$$T_n = \frac{T}{q\Phi_\omega} = \frac{m}{2q\Phi_\omega} \left(v_{x_0}^2 + v_{y_0}^2 \right) \quad (17)$$

For these plots, $a/b = 1.0$ and the angles ϕ are 0° , 30° and 60° . Note that only the trajectories for electrons leaving the plate within the limits $-a < y < a$ have been shown, due to the symmetry of the problem. The black circles at $x/b=1$ represent the line charges which repel the electrons.

By keeping track of the fraction of the electrons emitted from the unit cell that escape to infinity, it is possible to describe how well the grid behaves as a shield. In Figures 25 through 29, this fraction f is plotted as a function of T_n for various values of ϕ and a/b . In the present problem, this fraction is independent of the angle θ .

If from subsequent calculations, the spectral density of emitted electrons $n_e(T, \theta, \phi)$ is determined, the total number of electrons, N ,

escaping into the test volume may be determined by performing the integral

$$N = \int_0^{\infty} dT \int_{-\pi/2}^{\pi/2} d\phi \int_0^{\pi} d\theta n_e(T, \theta, \phi) f(T, \phi) \quad (18)$$

The spectral density of the electrons n_e , depends upon the energy of the incident gamma rays, the energy of the incident Compton electrons, and the properties of the cavity walls. This quantity will not be computed in this note.

In more general problems where the potential distribution is not simply a two dimensional function, but depends upon all of the cartesian co-ordinates, the fraction of escaping electrons will depend on θ as well as on ϕ and T . Nevertheless, Eq. (18) may be employed to determine the total number of escaping electrons for all angles and energies.

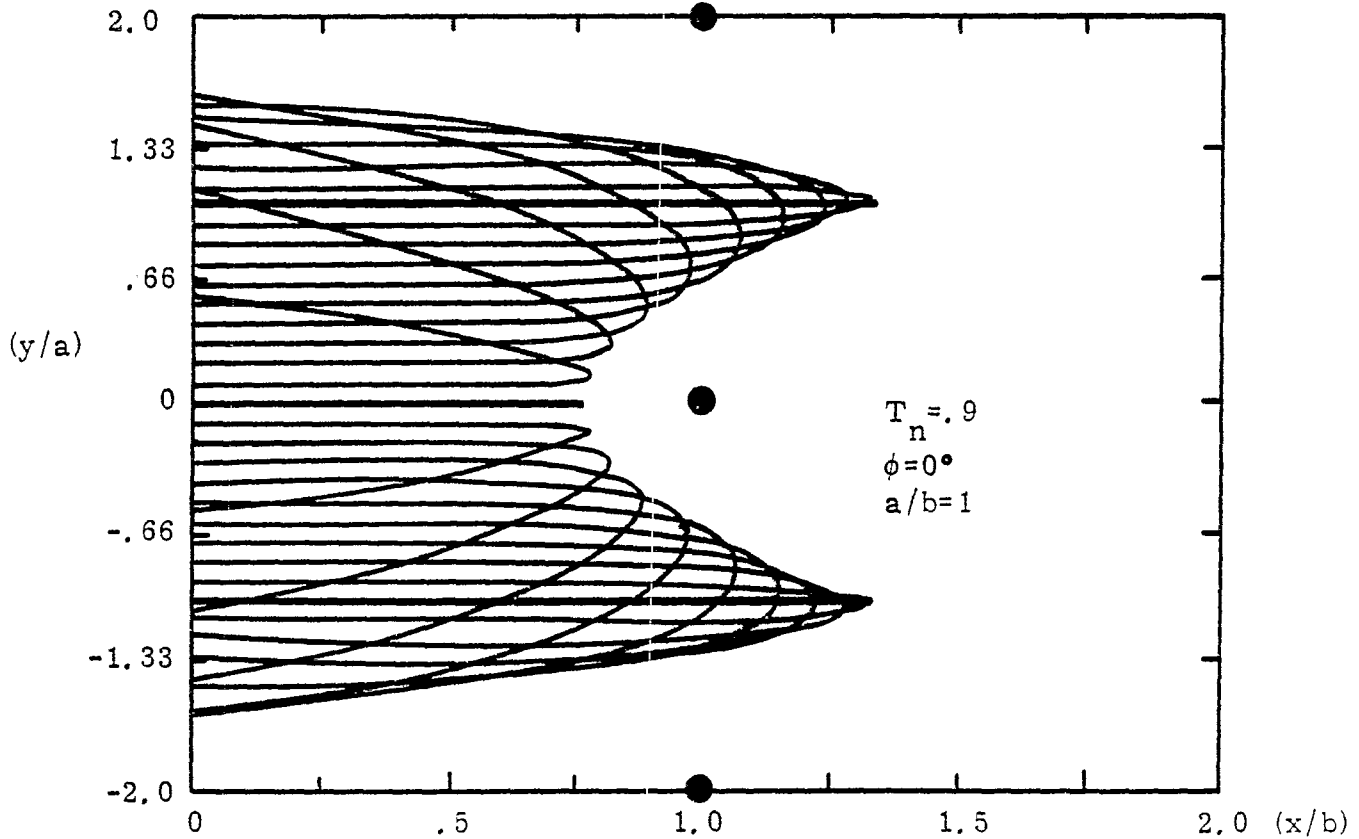
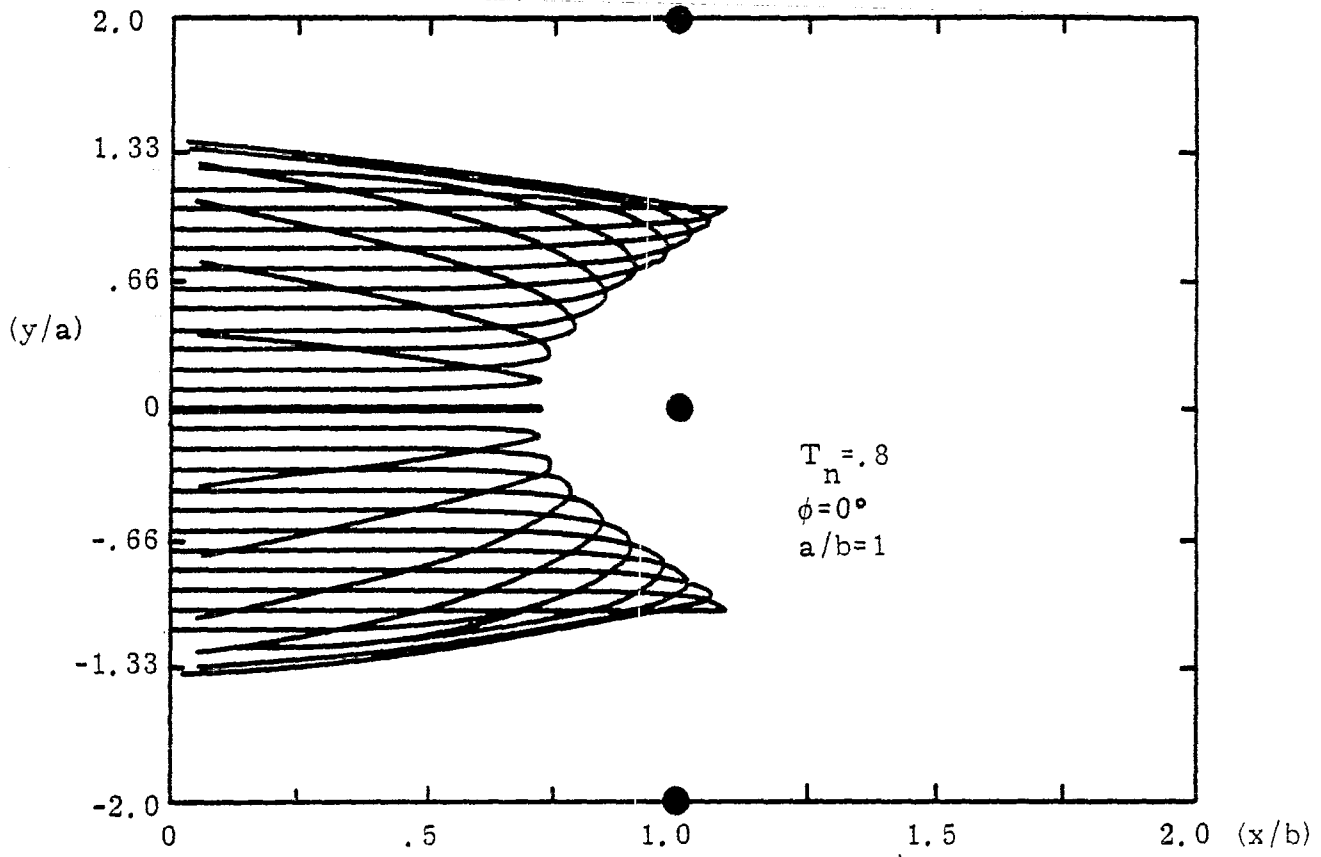


Figure 13. Trajectories of electrons leaving the ground plane at the angles $\theta = 90^\circ$, ϕ , within a unit cell.

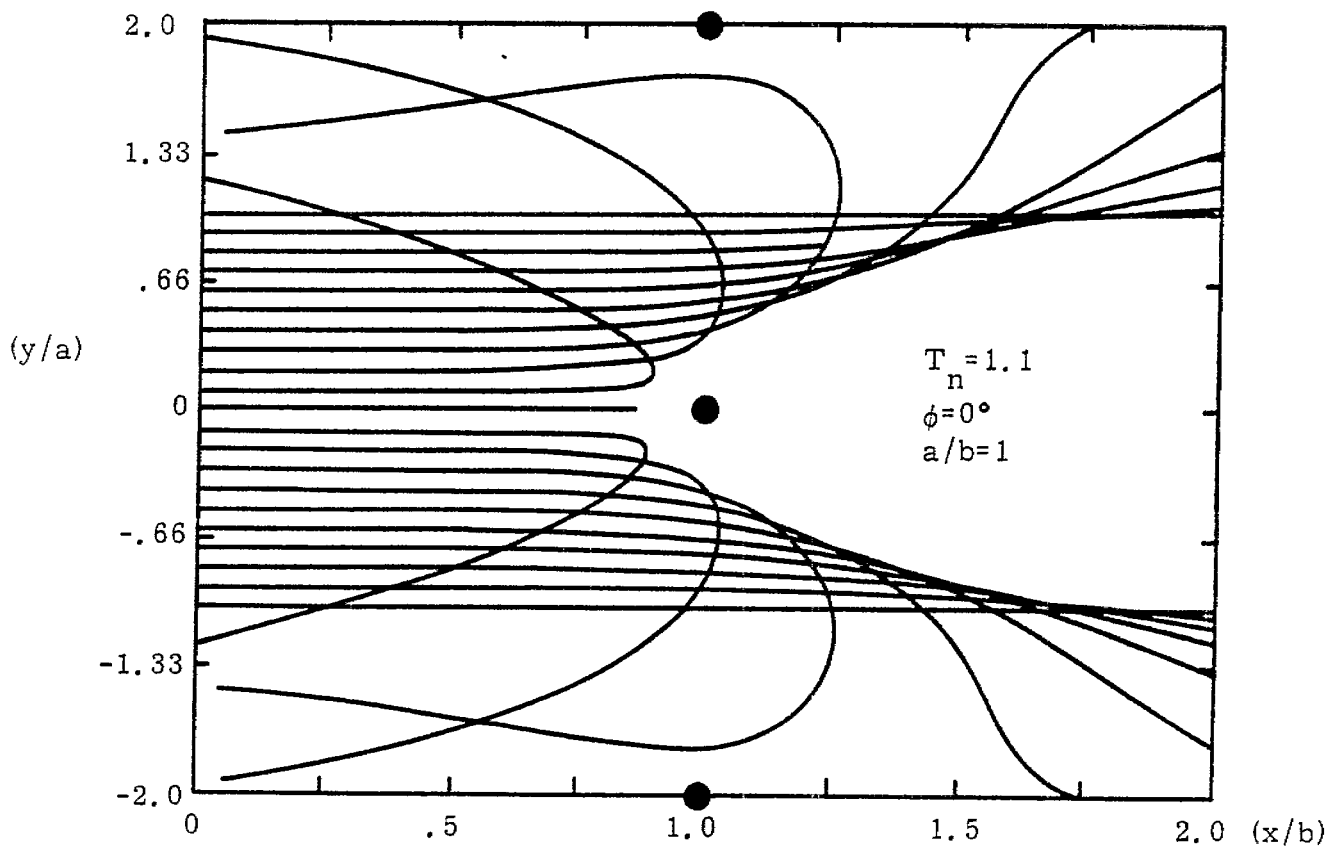
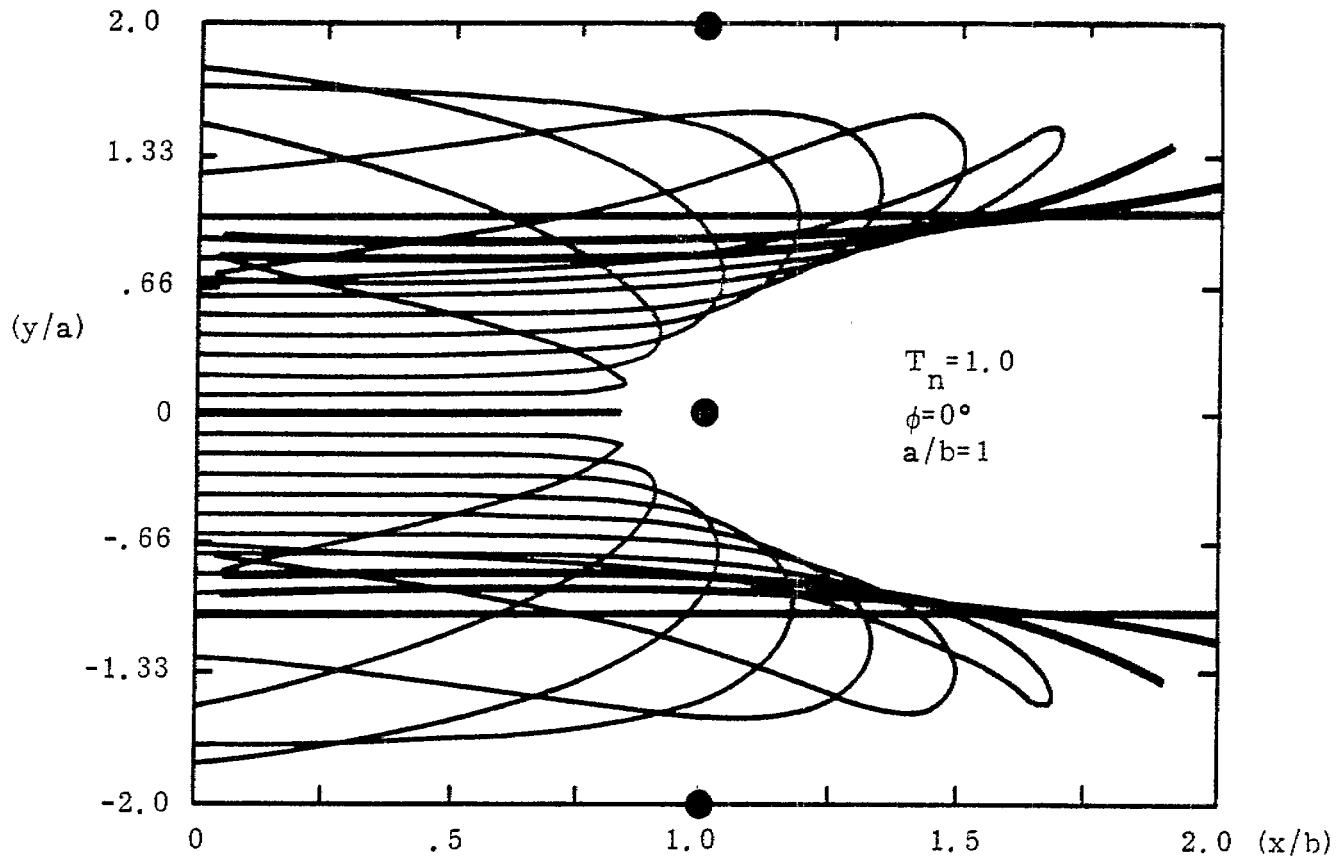


Figure 14. Trajectories of electrons leaving the ground plane at the angles $\theta = 90^\circ$, ϕ , within a unit cell.

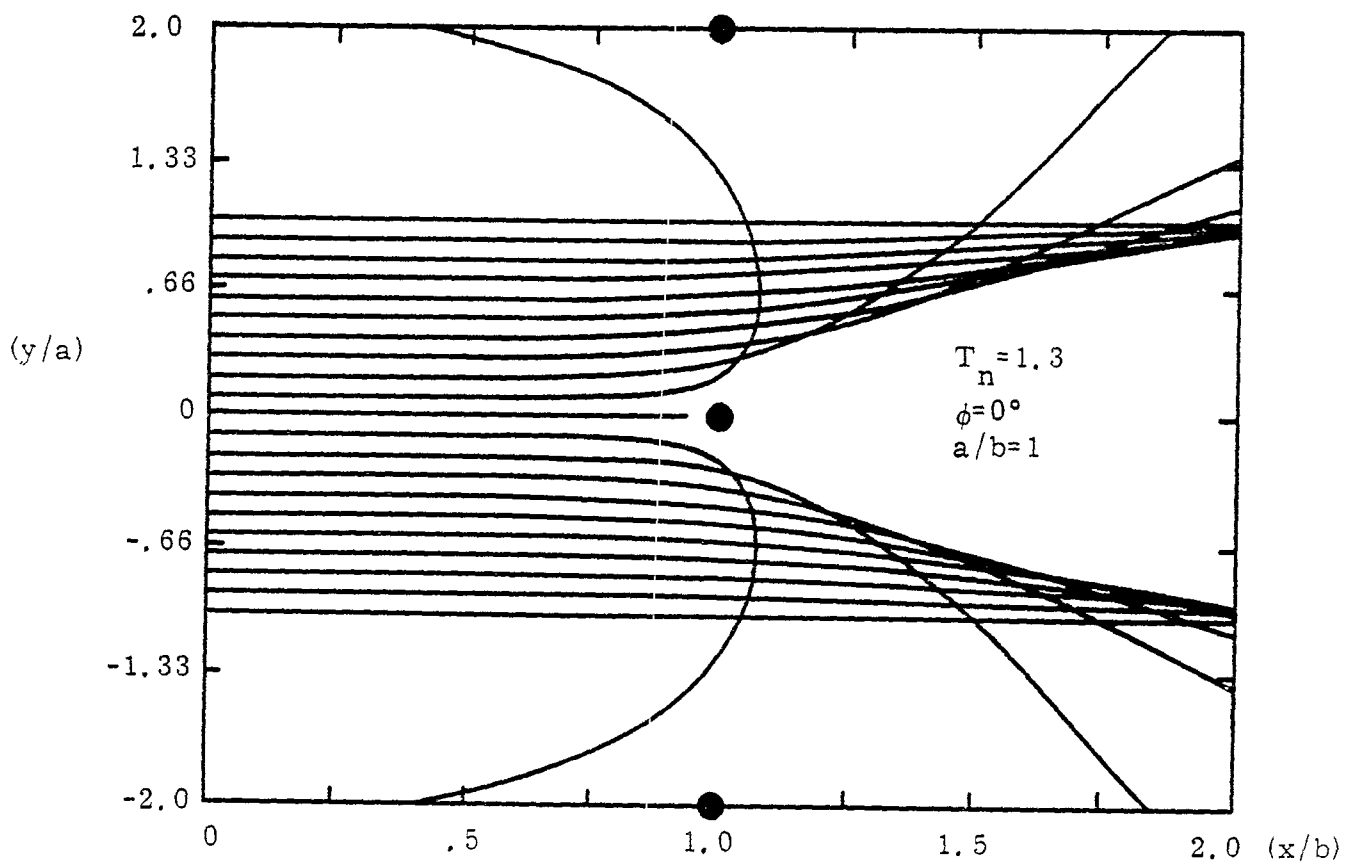
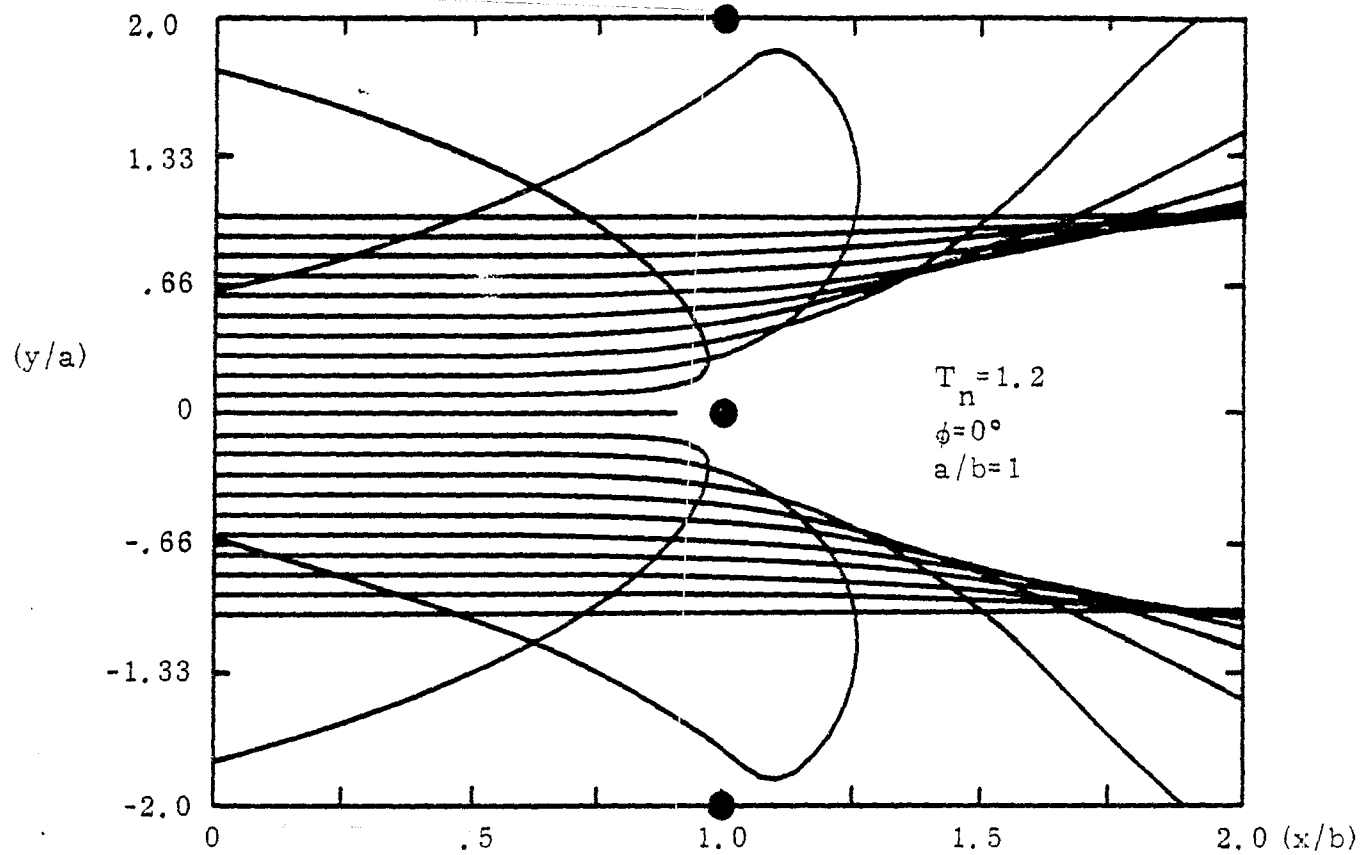


Figure 15. Trajectories of electrons leaving the ground plane at the angles $\theta = 90^\circ$, ϕ , within a unit cell.

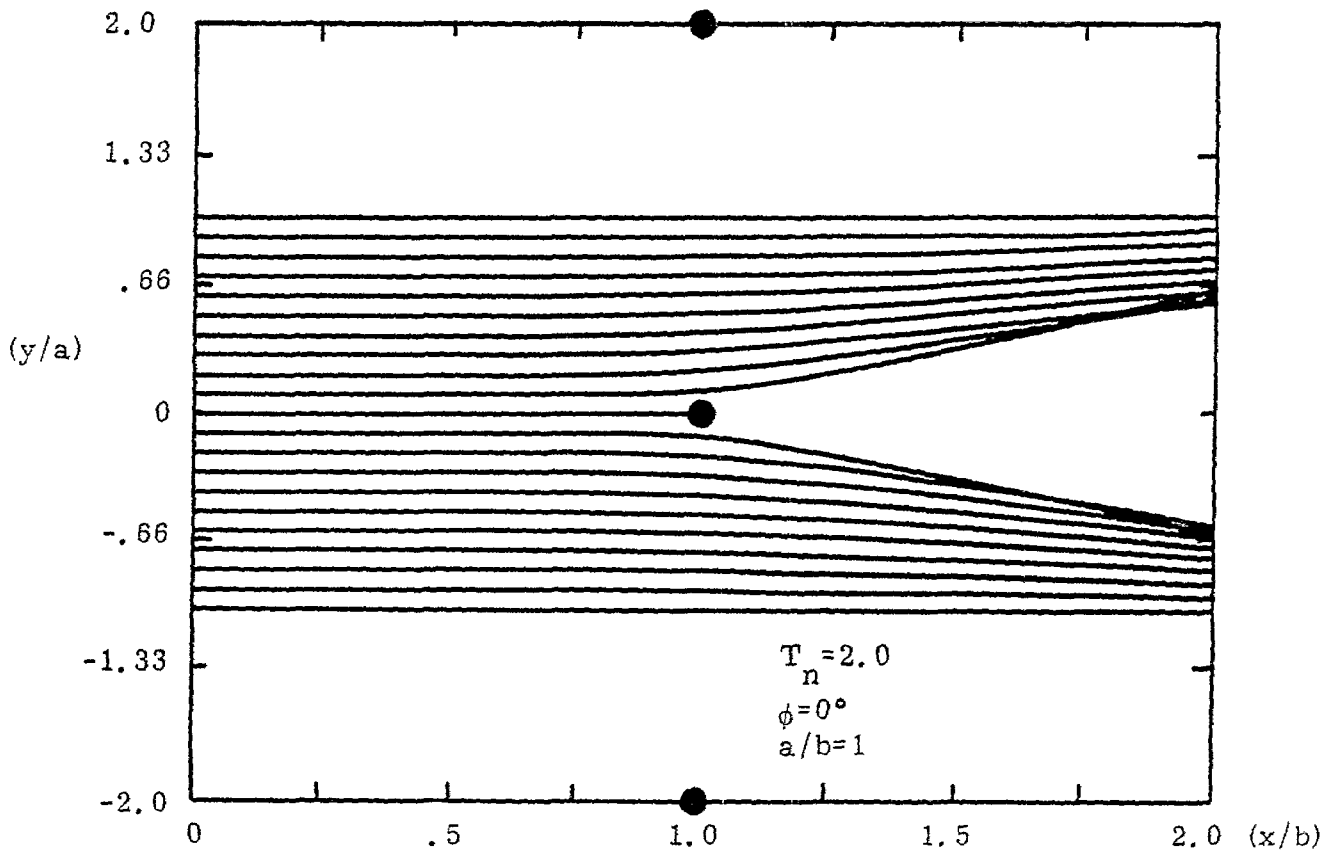
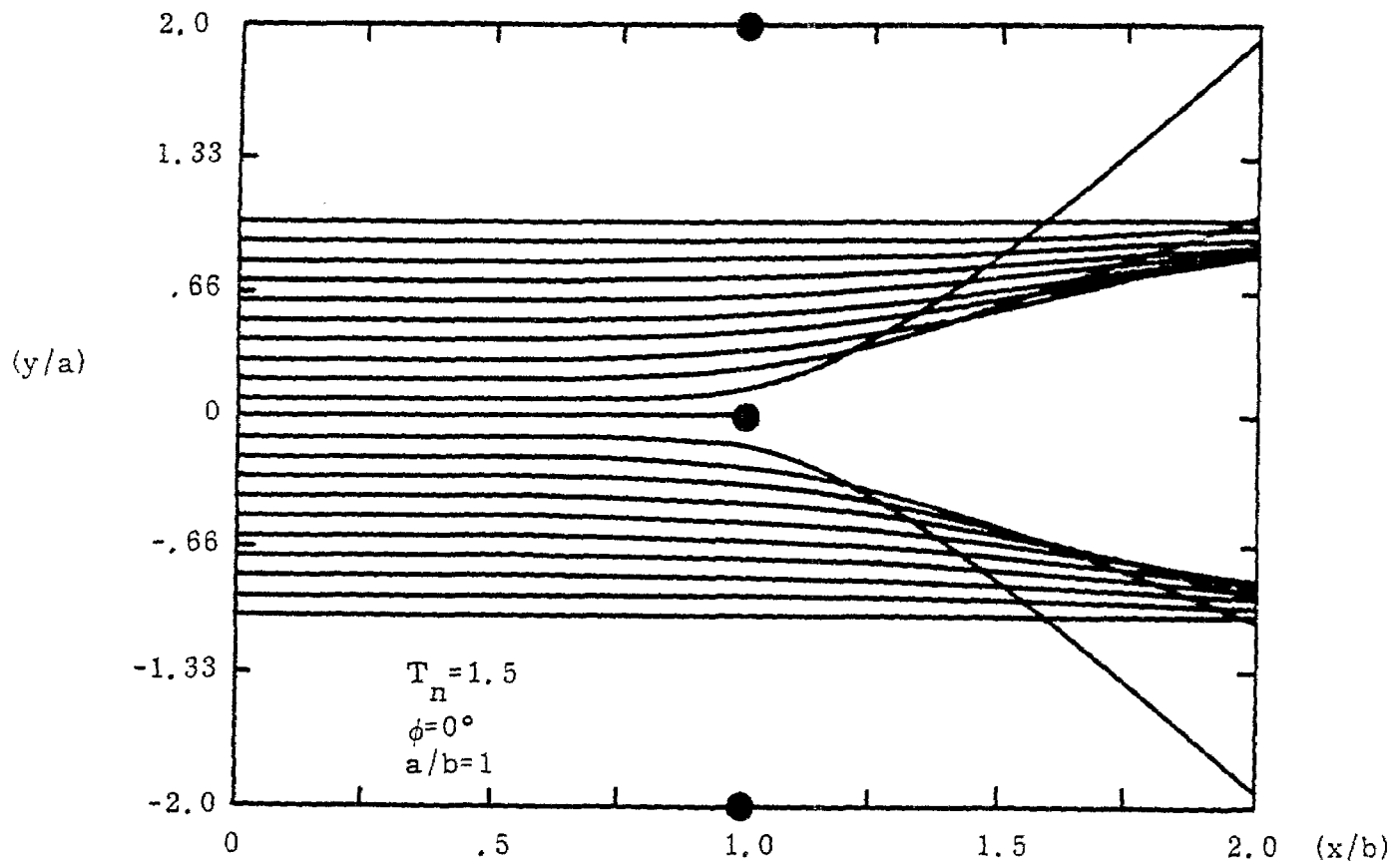


Figure 16. Trajectories of electrons leaving the ground plane at the angles $\theta = 90^\circ$, ϕ , within a unit cell.

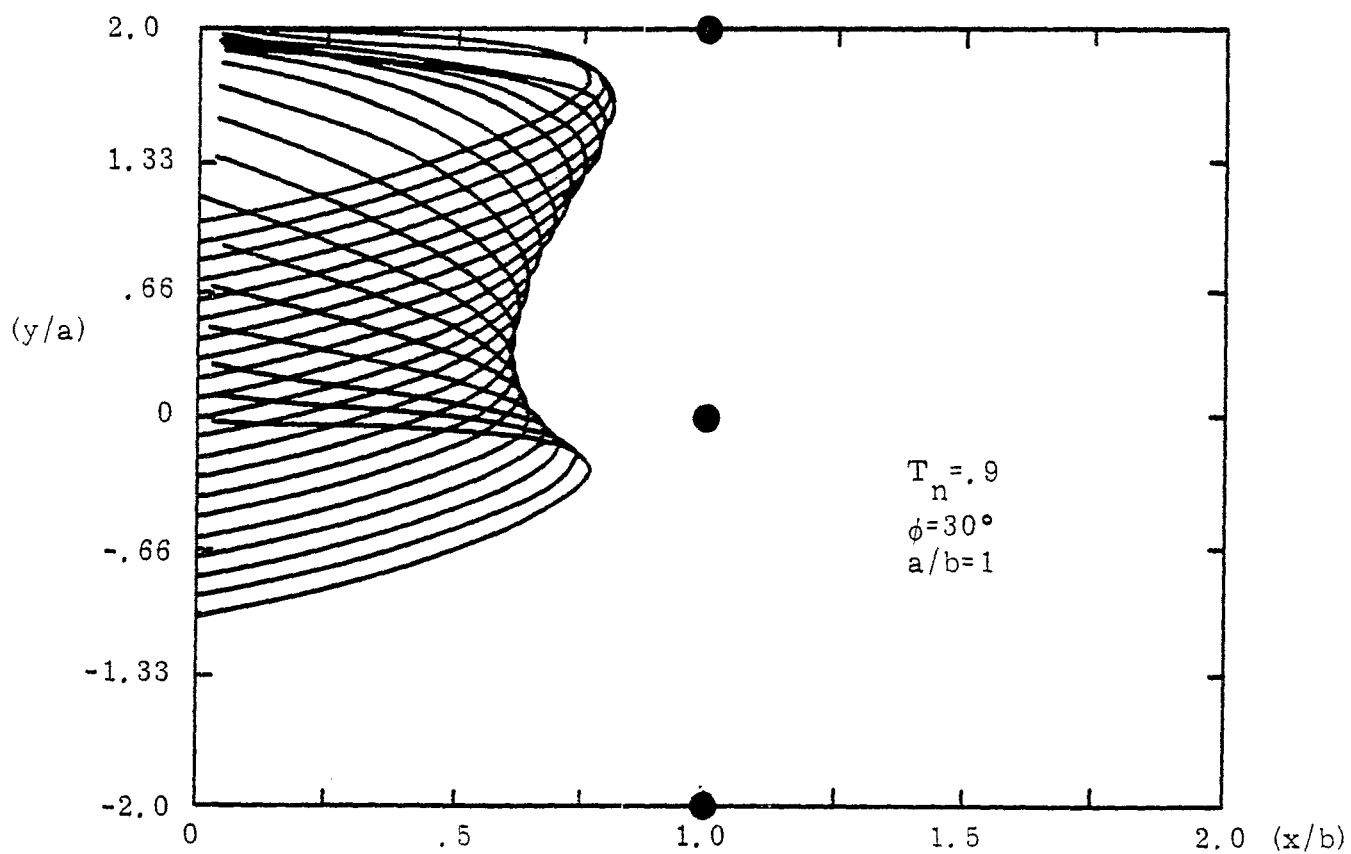
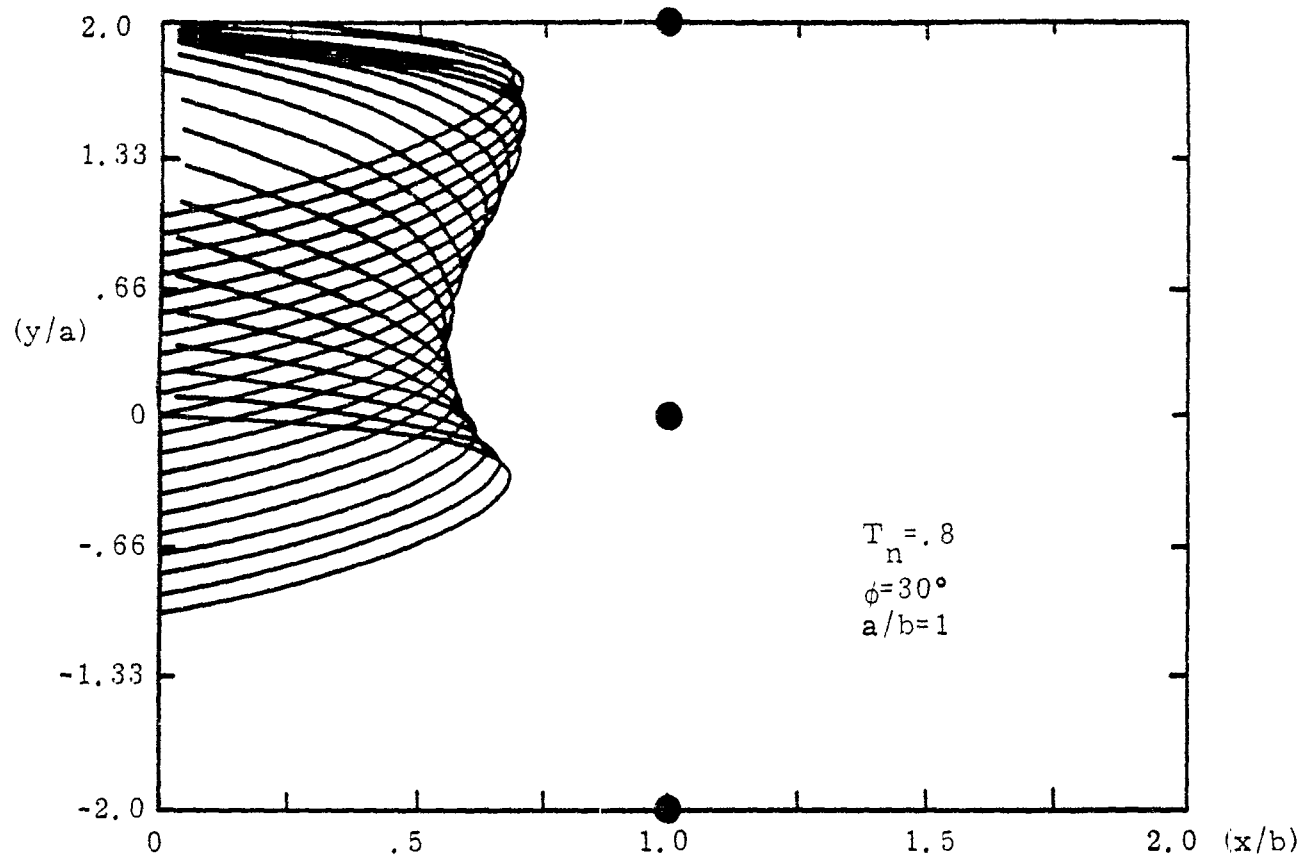


Figure 17. Trajectories of electrons leaving the ground plane at the angles $\theta = 90^\circ$, ϕ , within a unit cell.

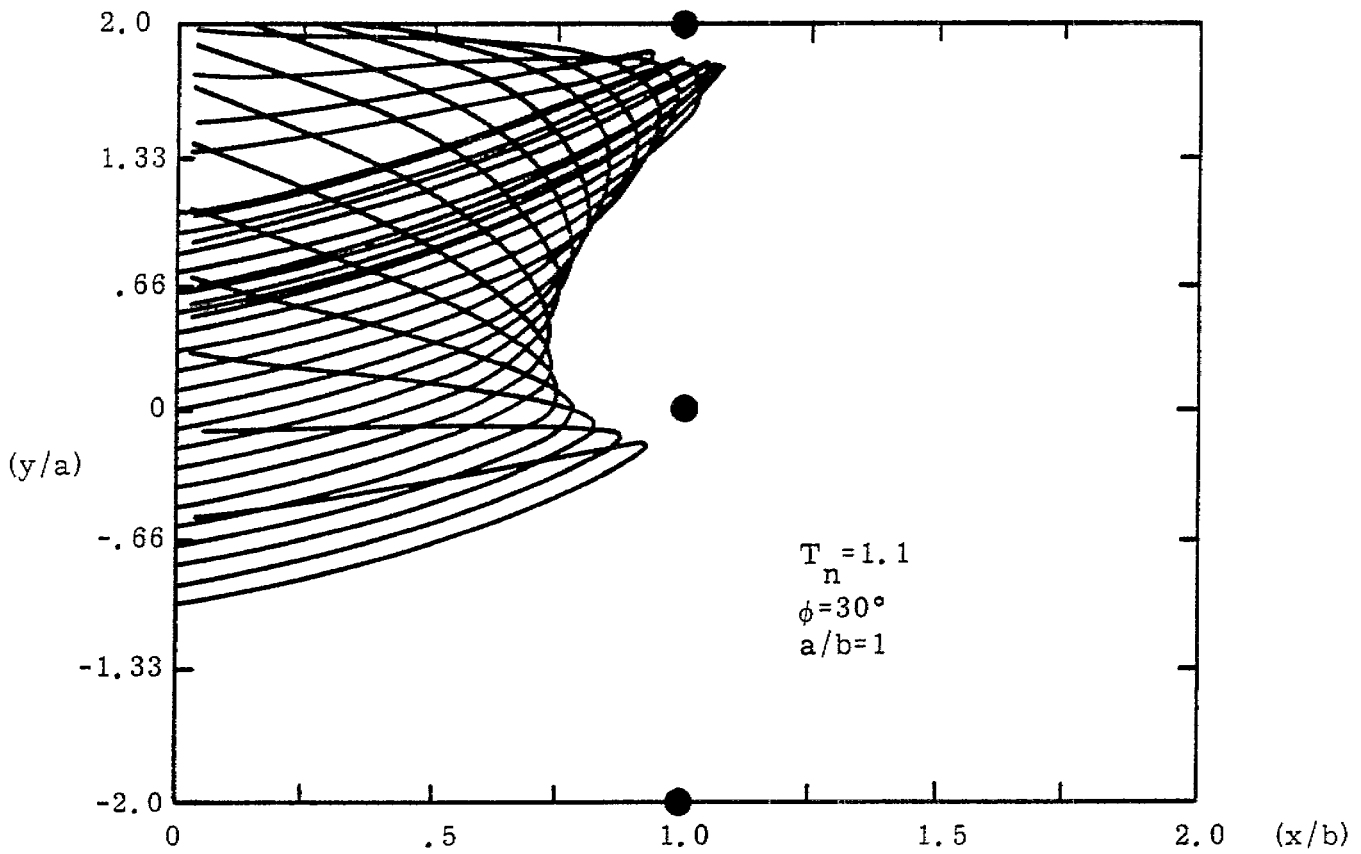
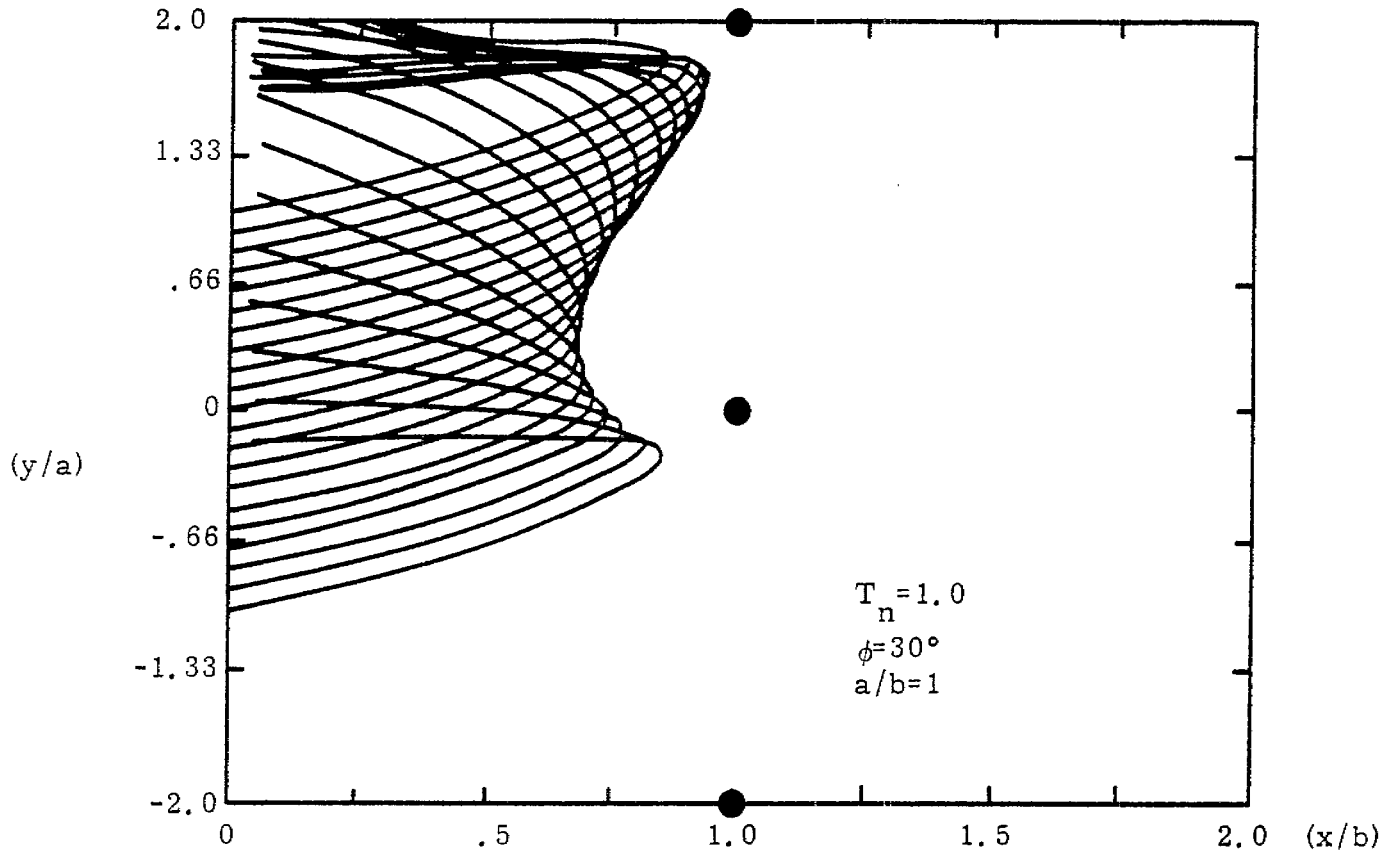


Figure 18. Trajectories of electrons leaving the ground plane at the angles $\theta = 90^\circ$, ϕ , within a unit cell.

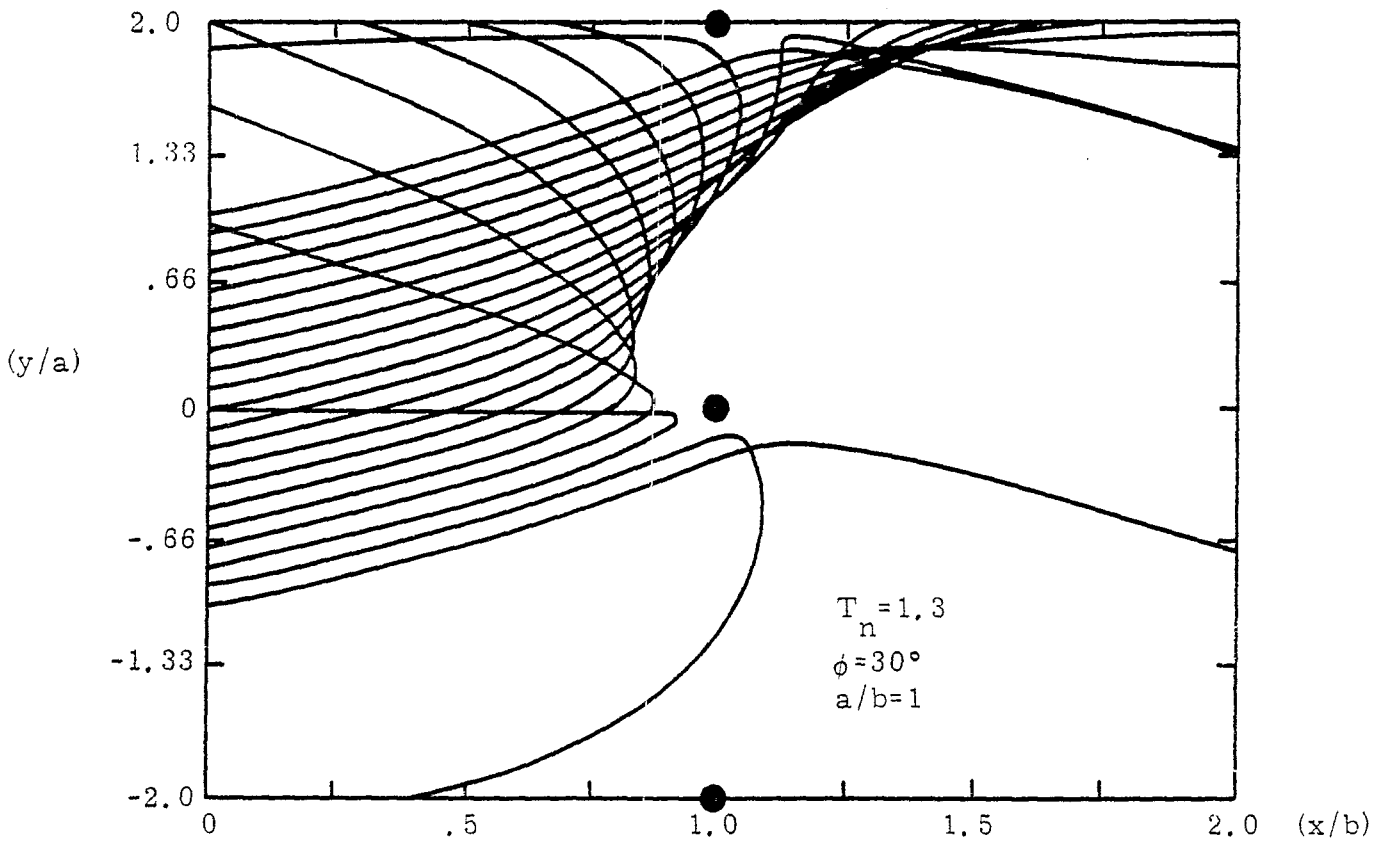
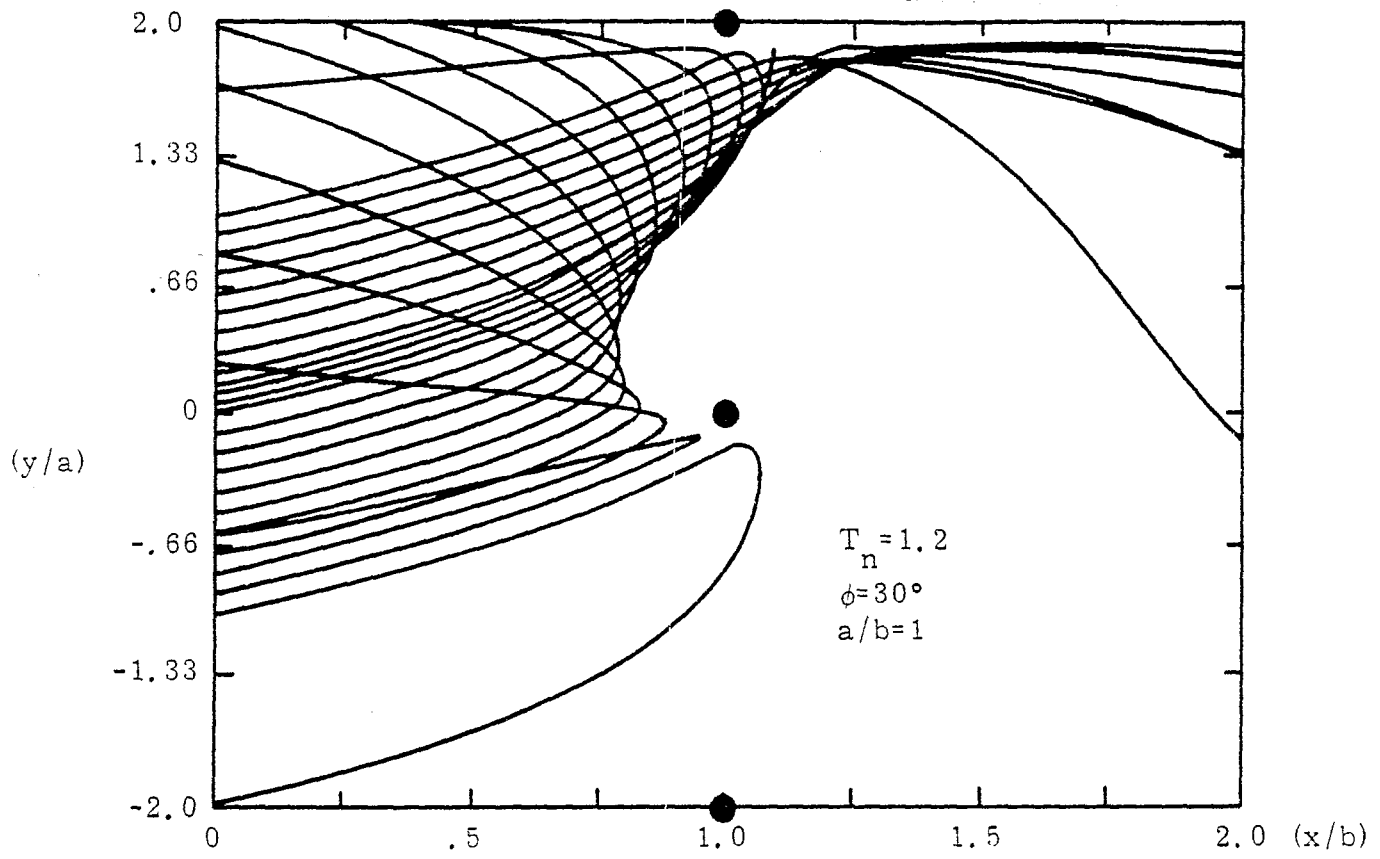


Figure 19. Trajectories of electrons leaving the ground plane at the angles $\theta = 90^\circ$, ϕ , within a unit cell.

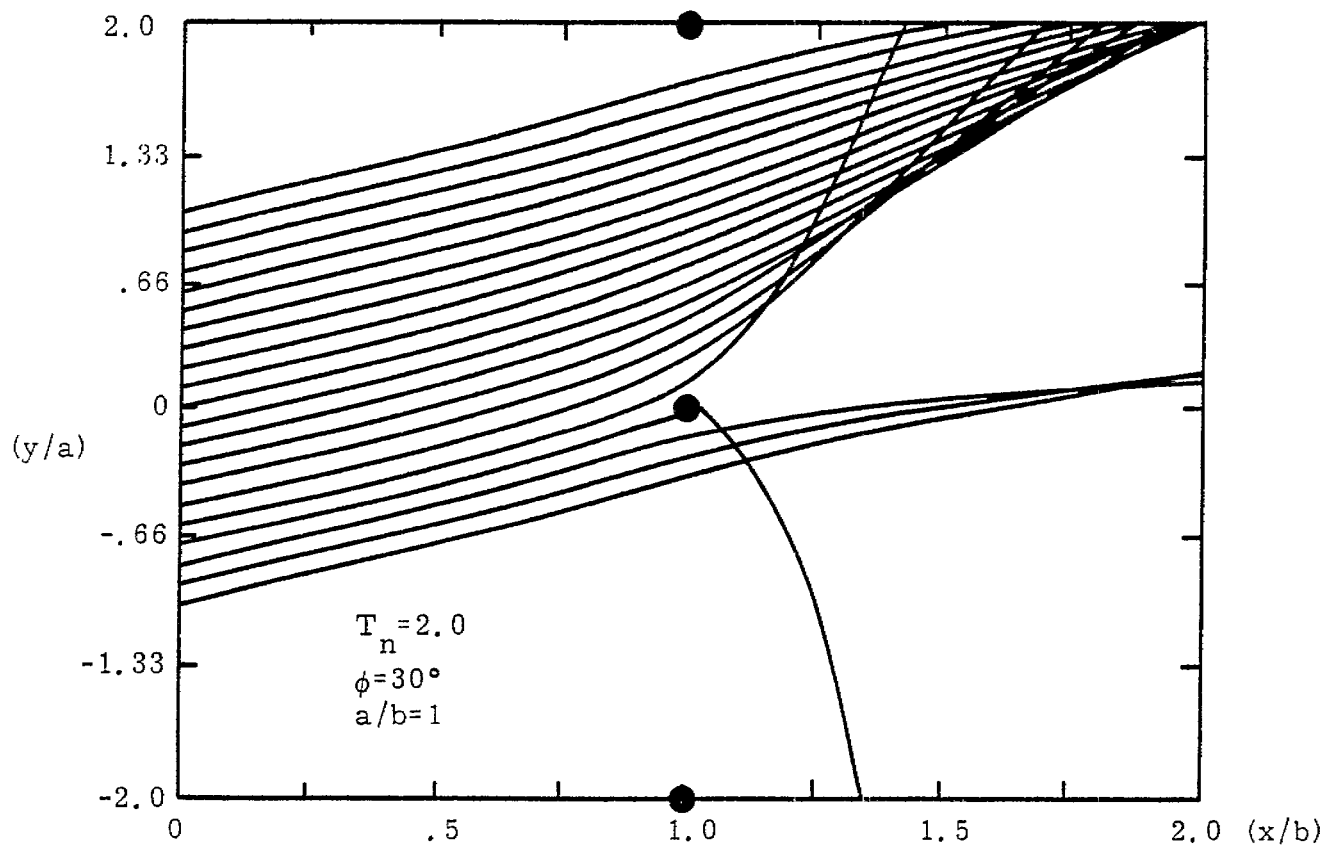
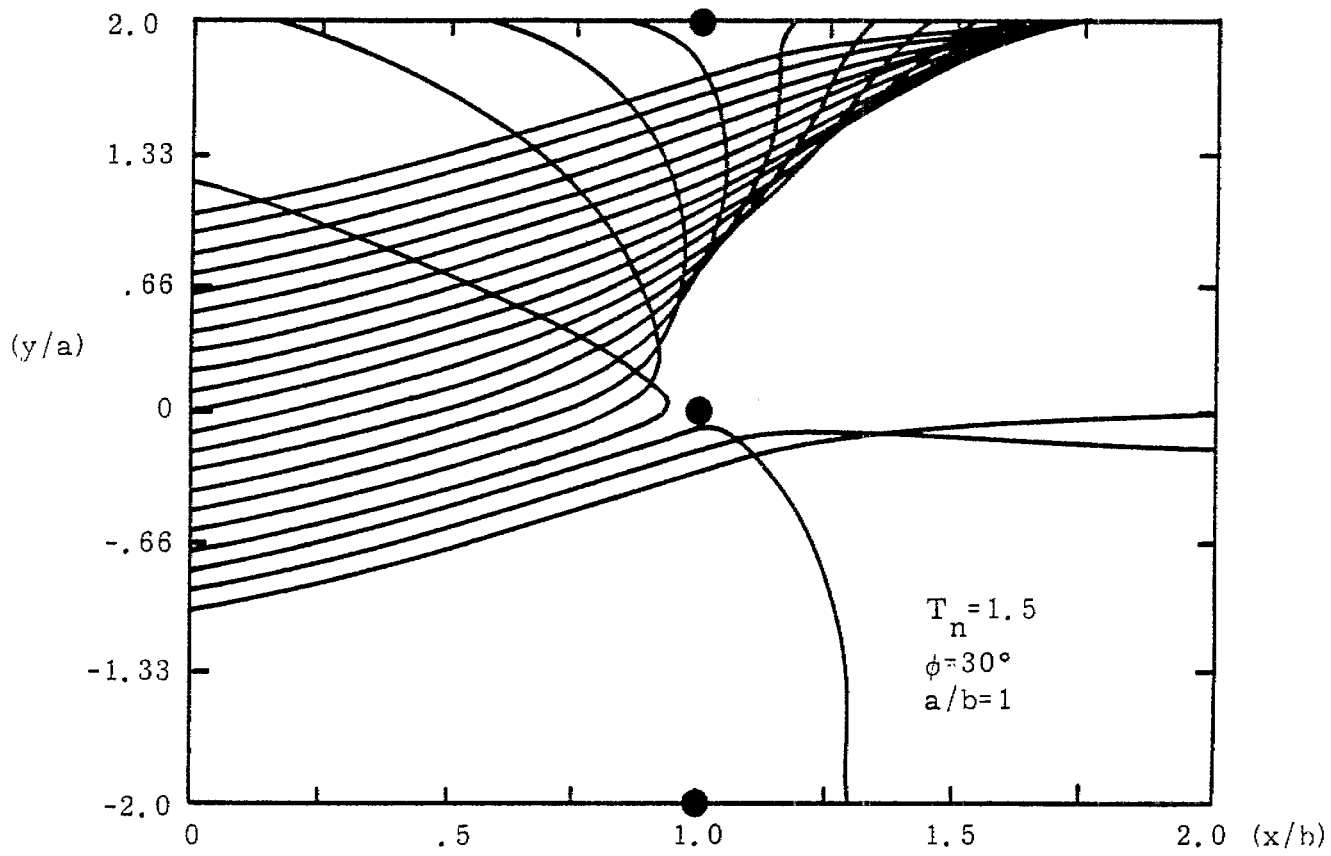


Figure 20. Trajectories of electrons leaving the ground plane at the angles $\theta = 90^\circ$, ϕ , within a unit cell.

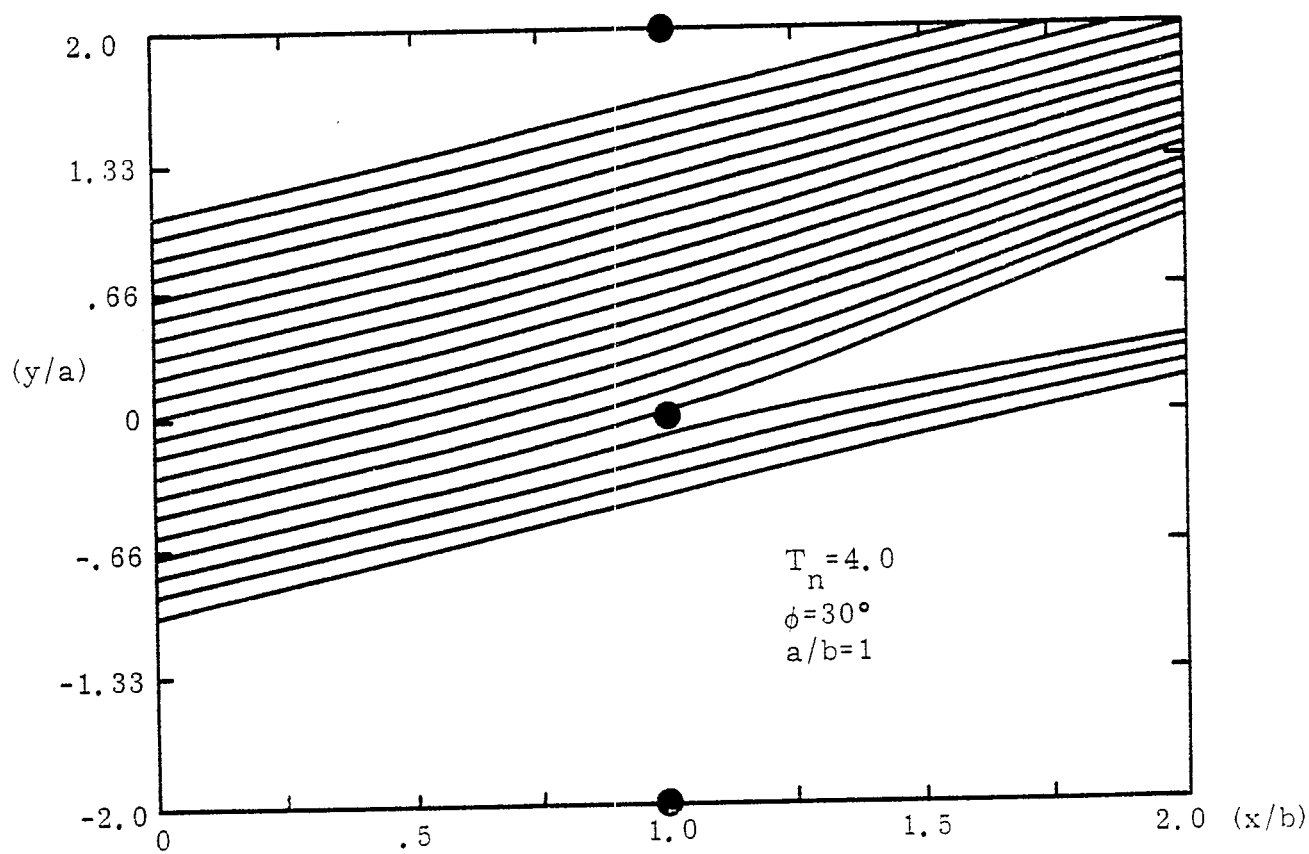
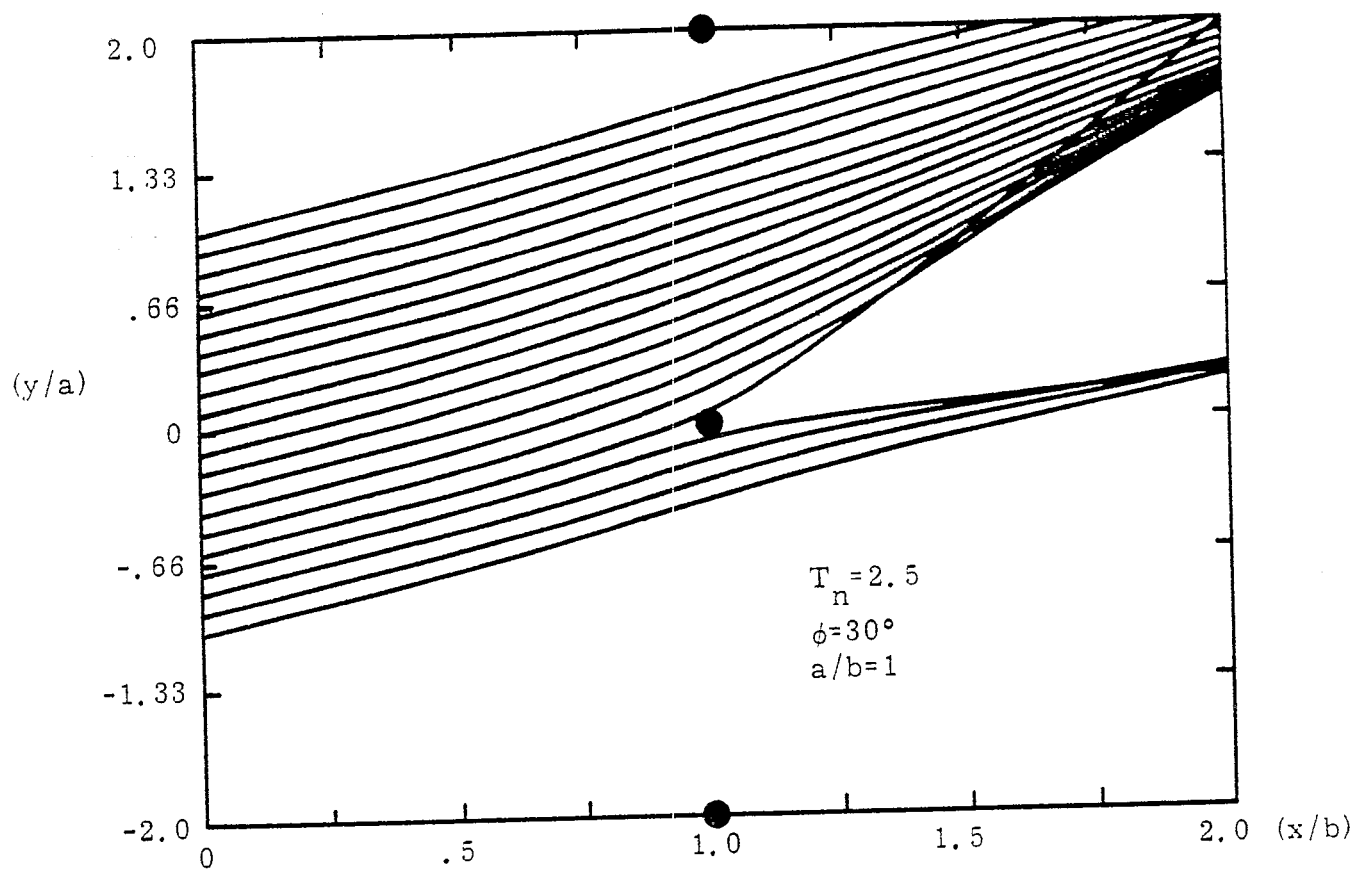


Figure 21. Trajectories of electrons leaving the ground plane at the angles $\theta = 90^\circ$, ϕ , within a unit cell.

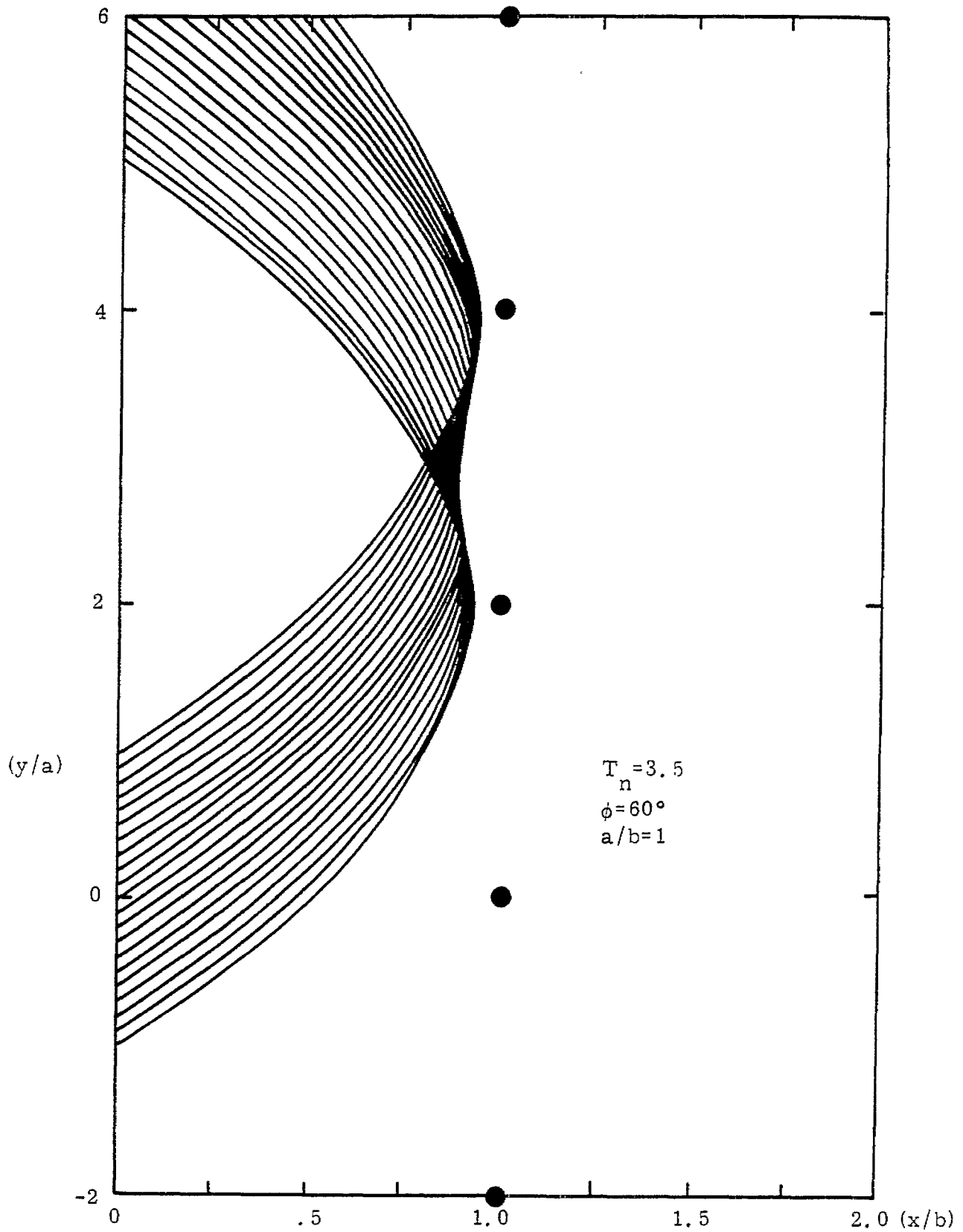


Figure 22. Trajectories of electrons leaving the ground plane at the angles $\theta = 90^\circ$, ϕ , within a unit cell.

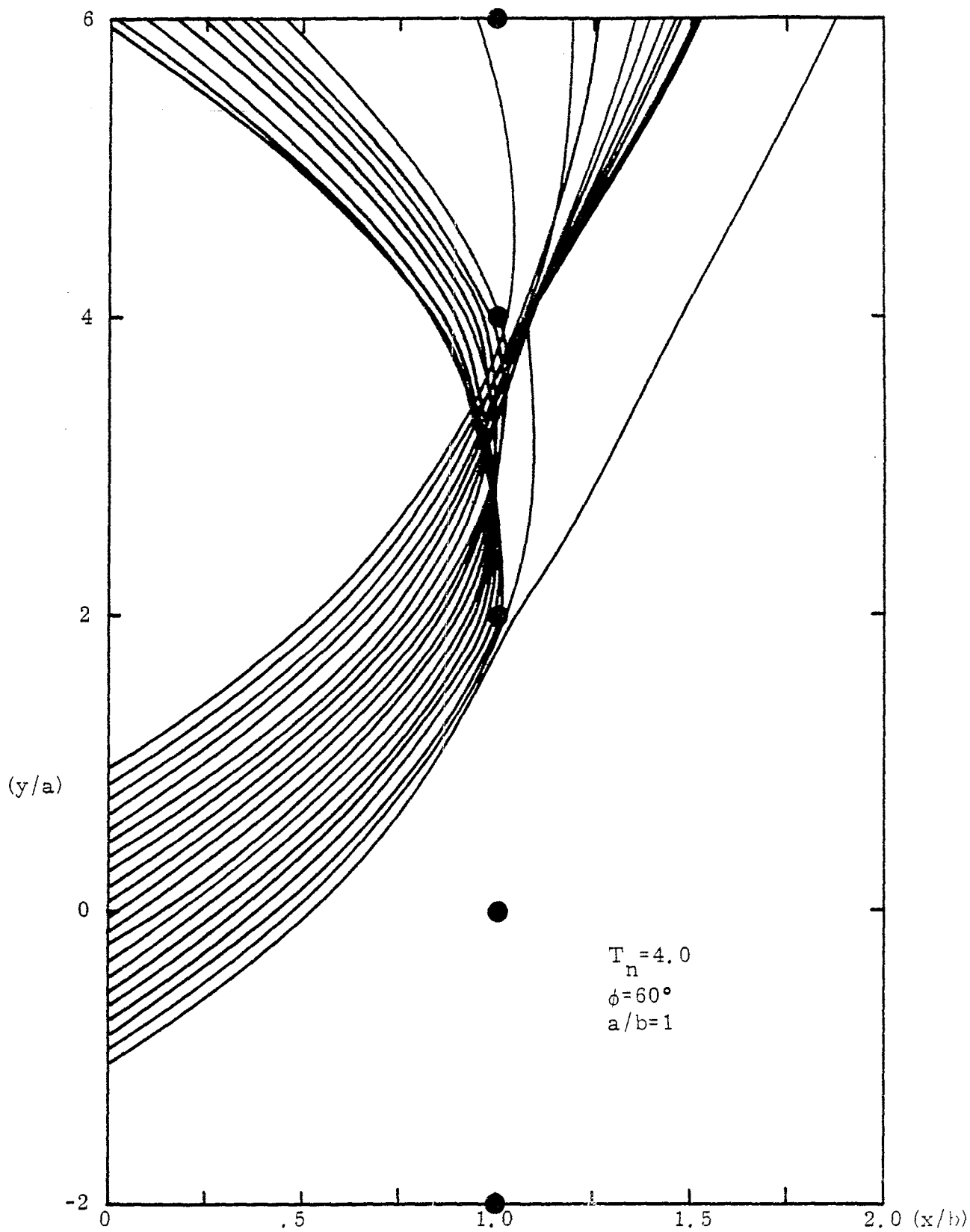


Figure 23. Trajectories of electrons leaving the ground plane at the angles $\theta = 90^\circ$, ϕ , within a unit cell.

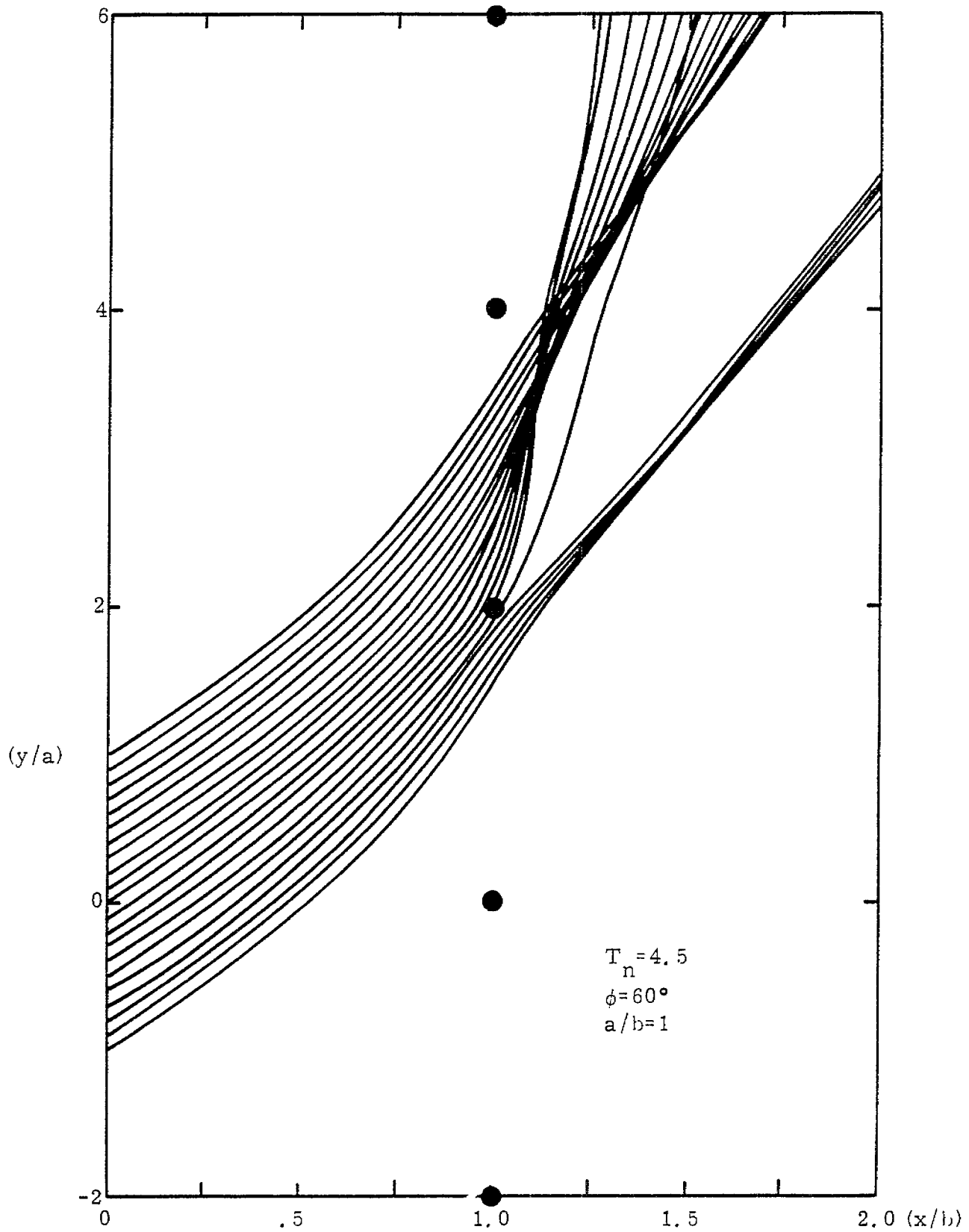


Figure 24. Trajectories of electrons leaving the ground plane at the angles $\theta = 90^\circ$, ϕ , within a unit cell.

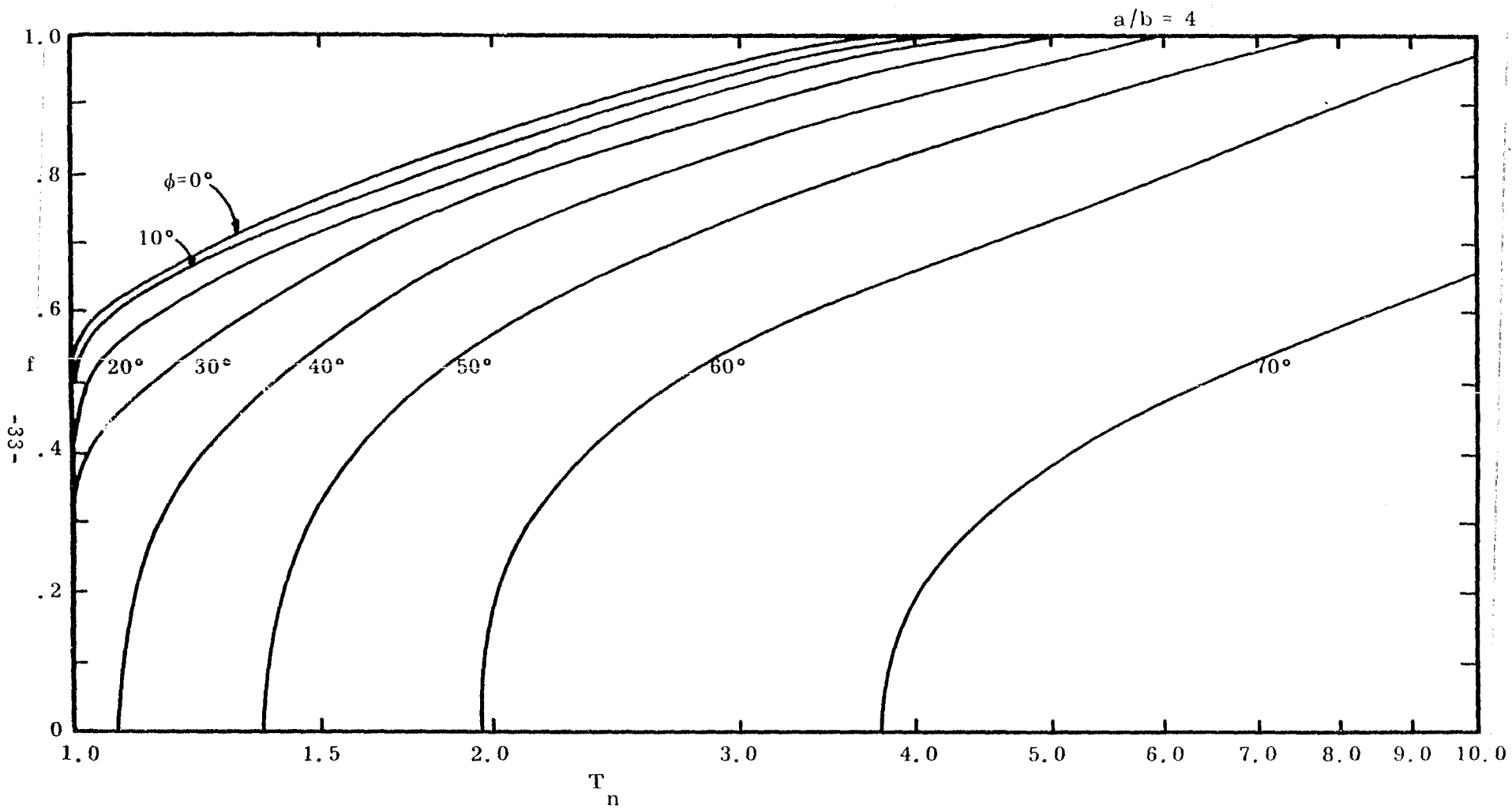


Figure 25. Plots of the fraction of electrons escaping to infinity as a function of normalized initial kinetic energy for various angles of departure.

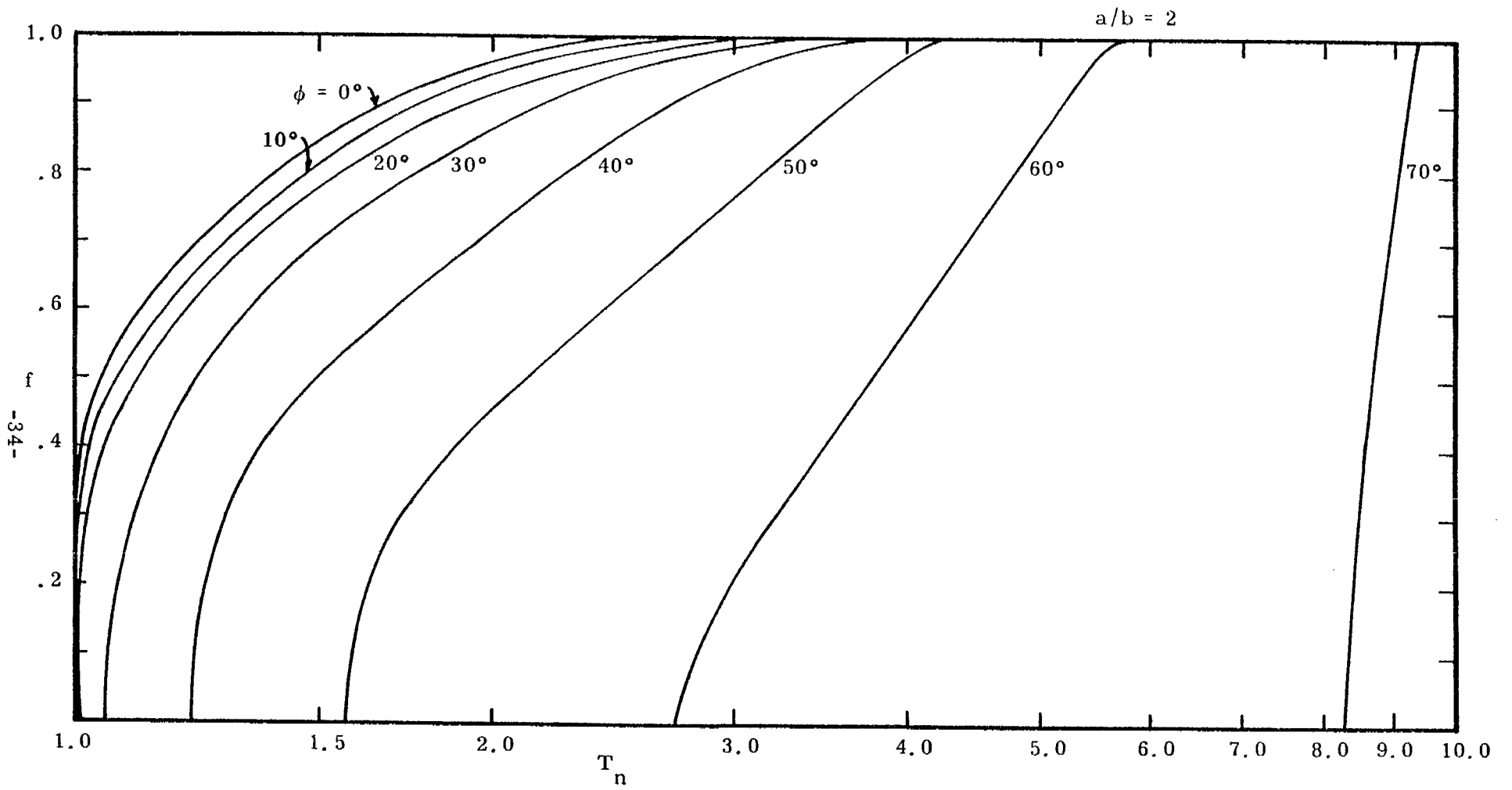


Figure 26. Plots of the fraction of electrons escaping to infinity as a function of normalized initial kinetic energy for various angles of departure.

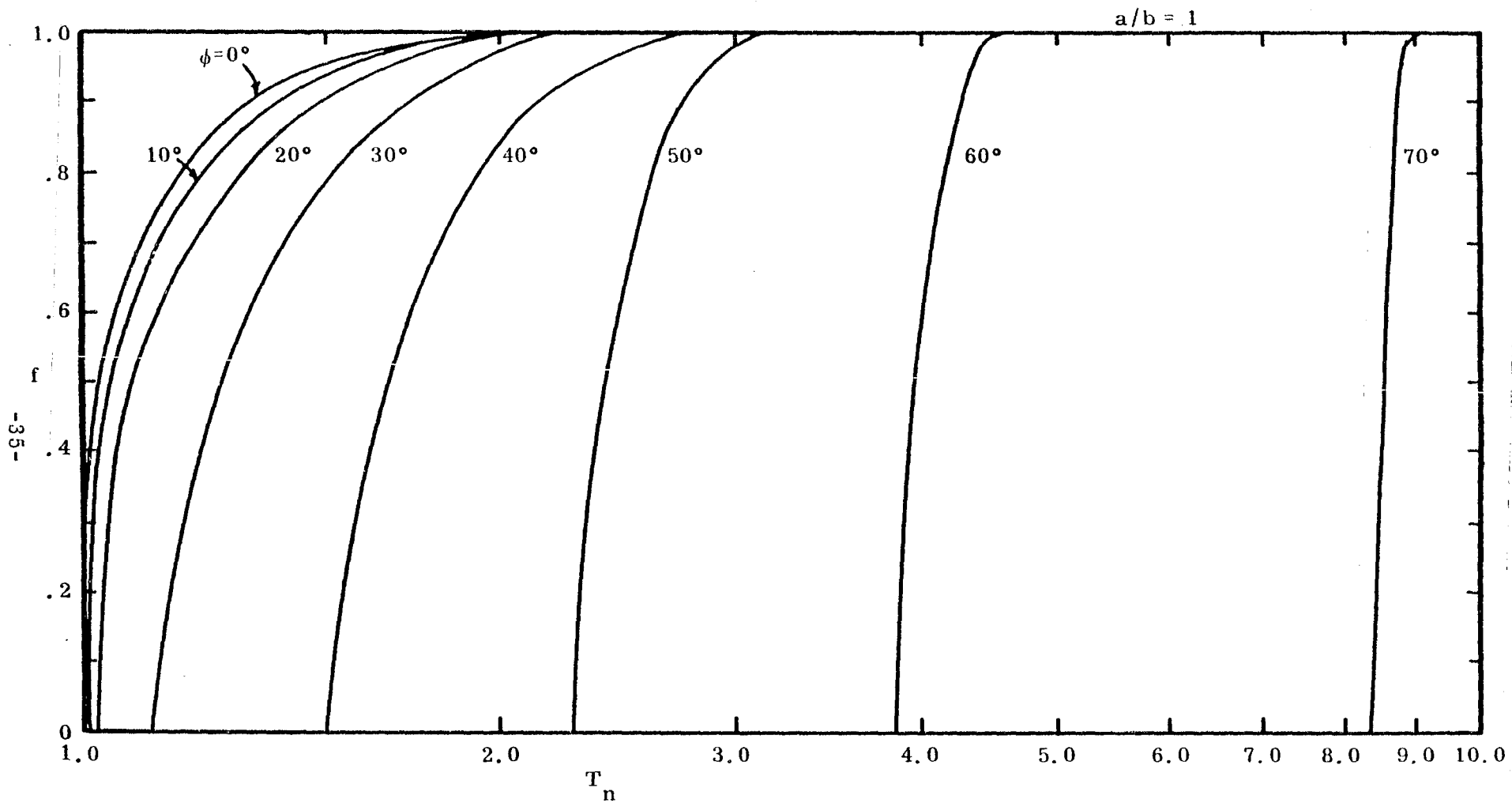


Figure 27. Plots of the fraction of electrons escaping to infinity as a function of normalized initial kinetic energy for various angles of departure.

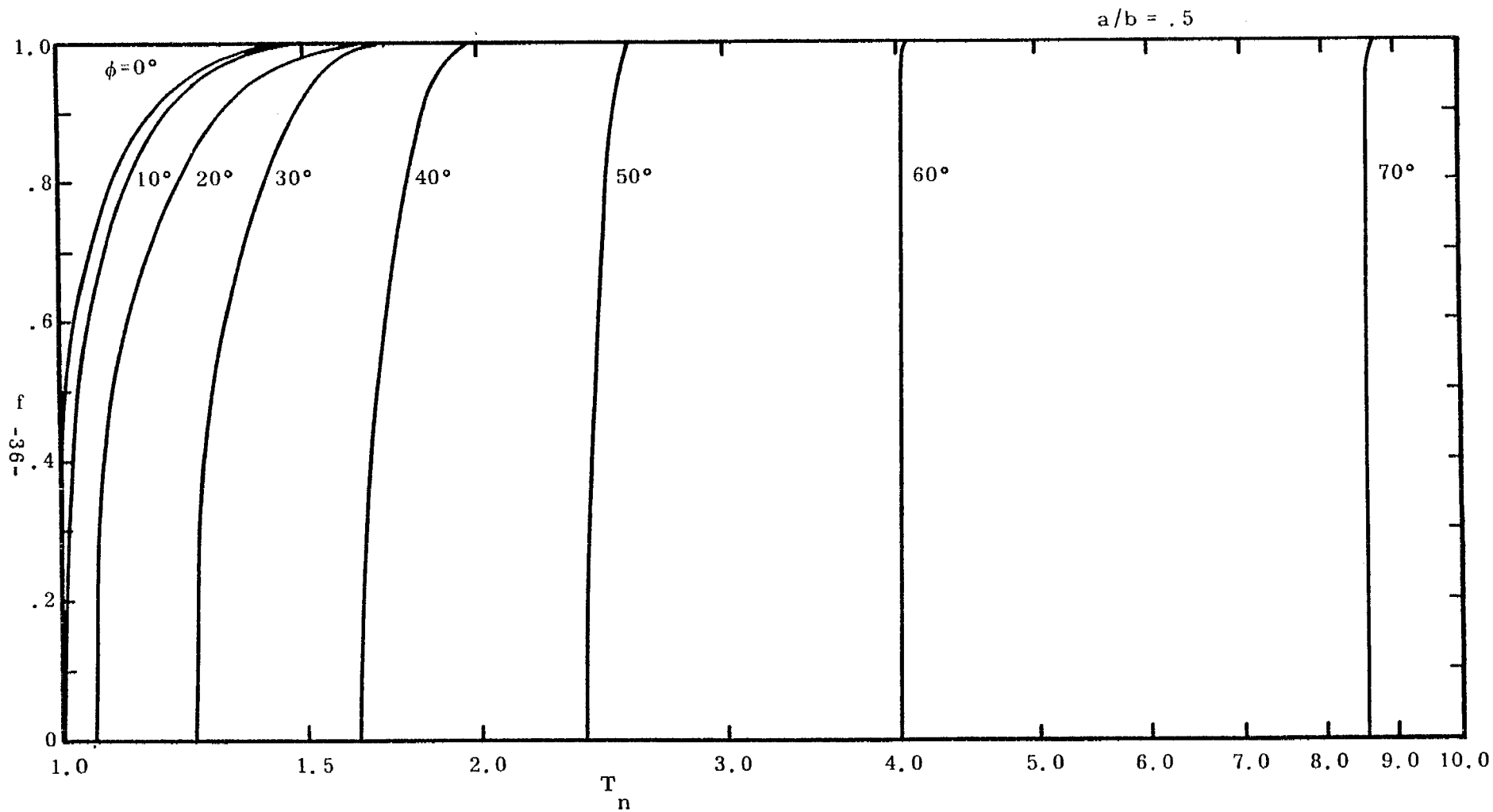


Figure 28. Plots of the fraction of electrons escaping to infinity as a function of normalized initial kinetic energy for various angles of departure.

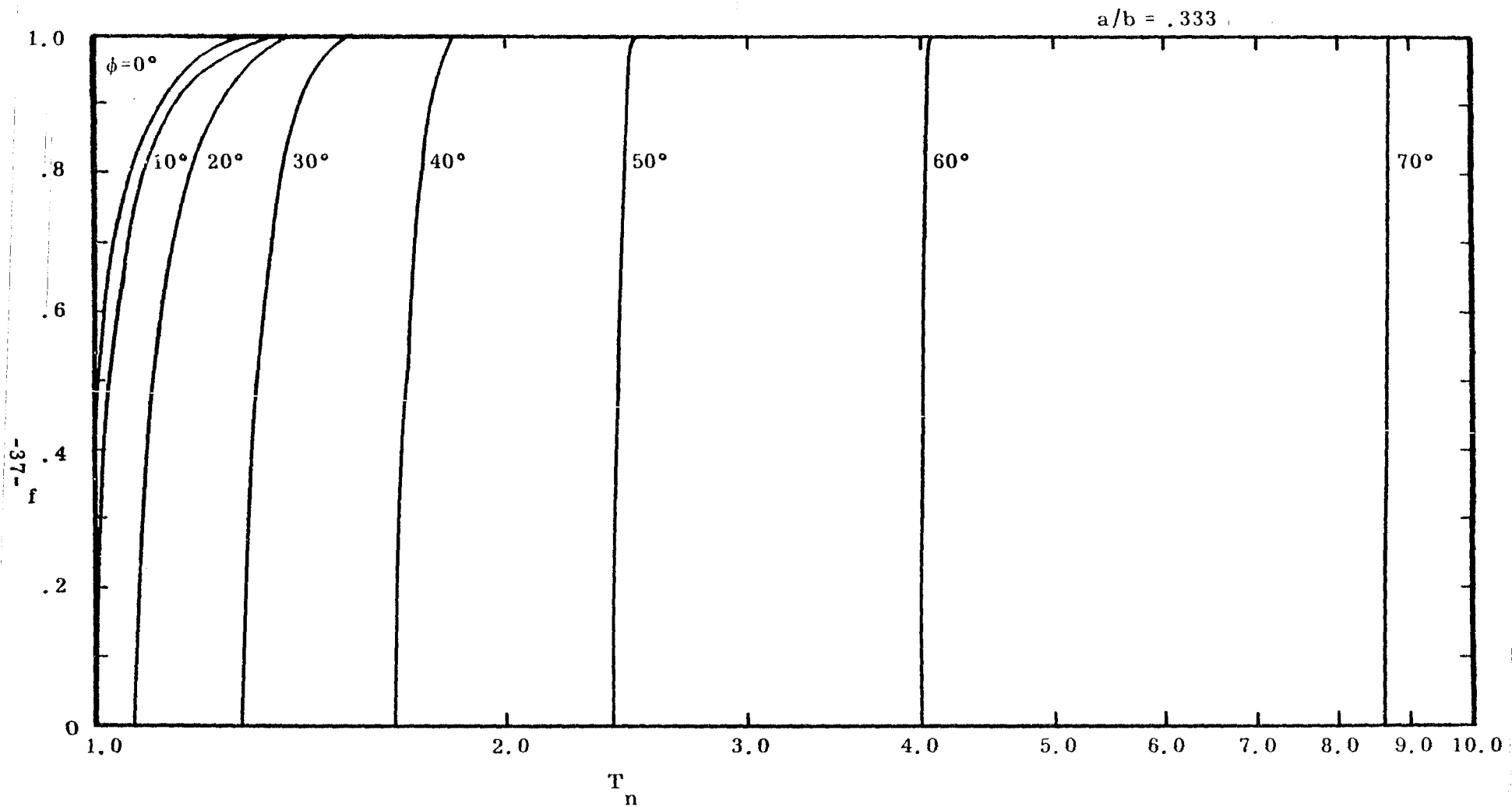


Figure 29. Plots of the fraction of electrons escaping to infinity as a function of normalized initial kinetic energy for various angles of departure.

IV. CONCLUSION

Using a conformal mapping technique, the potential distribution in space due to an infinite number of infinitely long charged cylinders located parallel to a ground plane was computed. From knowledge of the spatial distribution of potential, the trajectories of electrons being emitted from the ground plane have been calculated under the assumptions that the electrons are non-relativistic and that space charge effects are negligible.

By looking at the plots of the potential, very little real information is gained regarding the effectiveness of the grid as a shield for the back-scattered electrons. A more useful quantity is the fraction of electrons which manage to escape from the grid structure to infinity for a given initial kinetic energy and angle of departure from the wall.

From the curves of the fraction of electrons escaping, it is to be noted that the larger a/b ratios correspond to structures which apparently hinder the escape of those electrons leaving the plate with small angles ϕ . For small a/b , the reverse is true. The electrons leaving with large angles tend to be retarded more efficiently. In order to more accurately evaluate a practical design for a wire grid repeller for use in satellite simulators, it will be necessary to obtain the spectral density of the electrons emitted from the plate and perform the integrations indicated in Eq. 18.

V. REFERENCES

1. Baum, C. E., "A Technique for Simulating the System Generated Electromagnetic Pulse Radiating from an Exoatmospheric Nuclear Weapon Radiation Environment", SSN 156, September 1972.
2. Marin, Lennart, "Effect of Replacing One Conducting Plate of a Parallel-Plate Transmission Line by a Grid of Rods", SSN 118, October 1970.